

Unveiling the nature of Ultraluminous Infrared Galaxies with 3-4 μ m spectroscopy[†]

G. Risaliti,^{1,2} R. Maiolino,¹ A. Marconi,¹ E. Sani,³ S. Berta,⁴ V. Braito,⁵

R. Della Ceca,⁵ A. Franceschini,⁴ and M. Salvati¹

¹INAF - Osservatorio Astrofisico di Arcetri, L.go E. Fermi 5, I-50125 Firenze, Italy

²Harvard-Smithsonian Center for Astrophysics, 60 Garden st. Cambridge, MA

³Dipartimento di Astronomia, Università di Firenze, L.go E. Fermi 2, I-50125 Firenze, Italy

⁴Dipartimento di Astronomia, Università di Padova, Vicolo dell' Osservatorio 2, I-35122 Padova, Italy

⁵INAF - Osservatorio Astronomico di Brera, via Brera 28, I-20121 Milano, Italy

Released 2005 XXXXX XX

ABSTRACT

We present the results of L-band spectroscopical observations of local bright Ultraluminous Infrared Galaxies (ULIRGs), performed with ISAAC at the VLT. The excellent sensitivity of the telescope and of the instrument provided spectra of unprecedented quality for this class of objects, which allowed a detailed study of the AGN/starburst contribution to the energy output, and of the composition of the circumnuclear absorber. We discuss the L-band spectral features of seven single sources, and the statistical properties of a complete sample of 15 sources obtained combining our observations with other published 3-4 μ m spectra. Our main results are:

1. When a spectral indicator suggesting the presence of an AGN (low equivalent width of the 3.3 μ m emission line, steep $\lambda - f_\lambda$ spectrum, presence of an absorption feature at 3.4 μ m) is found, the AGN is *always* confirmed by independent analysis at other wavelengths. Conversely, in all known AGNs *at least* one of the above indicators is present.
2. Two new diagnostic diagrams are proposed combining the above indicators, in which starbursts and AGNs are clearly and completely separated.
3. The above diagnostic techniques are possible with spectra of relatively low quality, which can be obtained for several tens of ULIRGs with currently available telescopes. This makes L-band spectroscopy the current best tool to disentangle AGNs and starbursts contributions in ULIRGs.
4. The L-band properties of ULIRGs are heterogeneous. However, we show that all the spectral differences among ULIRGs can be reproduced starting from pure intrinsic AGN and starburst spectra and varying two parameters: the amount of dust extinction of the AGN component, and the relative AGN/starburst contribution to the bolometric luminosity.
5. Using the above decomposition model, we show that AGNs in ULIRGs have a low dust-to-gas ratio and a dust extinction curve different from Galactic.
6. The estimate of the presence and contribution of AGN in a complete sample show that AGN are hosted by $\sim 2/3$ of ULIRGs, but their energetic contribution is relevant ($> 30\%$ of the bolometric luminosity) only in $\sim 20\%$ of the sample.

Key words: galaxies: active – galaxies: starburst – infrared: galaxies

1 INTRODUCTION

Ultraluminous Infrared Galaxies (ULIRGs, $L_{IR} > 10^{12} L_\odot$) are the most luminous sources in the local Universe. More-

over, they represent the local counterparts of the class of high redshift objects dominating the far-infrared (FIR) and sub-mm backgrounds (Sanders & Mirabel 45 and references therein). Understanding the origin of the huge infrared emission of ULIRGs is therefore important in itself, given the relevance of this class of objects in the low redshift Universe, and in order to understand the nature of the high redshift

[†] Based on observations collected at the European Southern Observatory, Chile (proposals ESO 69.A-0643, ESO 73.B-0574).

FIR sources, which are too faint to be studied in detail with current instrumentation (even if the Spitzer Space Telescope is a major improvement in this direction, Werner et al. 57).

These considerations prompted a large interest in observational and theoretical studies on this class of sources. The main well established aspects on the physics of ULIRGs are: (a) the infrared (from a few μm to $\sim 1000 \mu\text{m}$) emission dominates the total luminosity, and is due to dust reprocessing of higher frequency radiation¹; (b) ULIRGs are mainly found in interacting or highly irregular systems (Sanders et al. 44).

Two different physical processes are possible as the primary energy source of ULIRGs: nuclear activity due to gas accretion onto a supermassive black hole and/or strong starburst activity. Several studies have been performed in the past 20 years, with the aim of understanding (a) which fraction of ULIRGs host an AGN, and (b) which is the contribution of the AGN to the bolometric luminosity.

In the optical and near-IR, spectral classification of ULIRGs of the IRAS 1 Jy sample (Kim & Sanders 24) established that only a minor fraction of ULIRGs have a clear signature of an AGN (Veilleux et al. 52, Veilleux, Kim, & Sanders 53, Veilleux, Sanders, & Kim 54). This fraction increases with luminosity from $\sim 20\%$ for objects with luminosity in the range $L_{IR} \sim 10^{11} - 10^{12} L_\odot$ to $\sim 50\%$ for objects with $L_{IR} > 10^{12.3} L_\odot$ (Veilleux et al. 52). A large fraction ($\sim 40\%$) of ULIRGs in the 1 Jy sample have optical/near-IR spectra typical of Low Ionization Narrow Emission Regions (LINERs). This classification leaves the question about the starburst/AGN relative contribution open.

In the mid-IR, ISO spectra of bright ULIRGs provided a powerful diagnostics for the study of the nature of these sources (Genzel et al. 14, hereafter G98). The presence of high ionization coronal lines in the mid-IR has been proven to be an indicator of the presence of an AGN (G98, Lutz et al. 30), while the presence of strong emission features due to polycyclic aromatic hydrocarbon (PAH) molecules is an indication of starburst dominance (see next Section for further details).

In the X-rays, spectra of bright ULIRGs, obtained with *XMM-Newton* by our group (Franceschini et al. 13, Braito et al. 5, Braito et al. 6) and with *Chandra* (Ptak et al. 35) revealed the capability of hard X-ray spectroscopy to disentangle the contributions of starbursts and AGNs.

The works briefly referred to above significantly enhanced our understanding of the nature of the emission of ULIRGs, but still have relevant limitations, which can be divided into two classes:

(a) Reliability of the diagnostic techniques. Most of the AGN indicators fail in several cases to detect an existing AGN, if this is heavily obscured by gas and dust. An extreme example of such limitations is the ULIRG NGC 6240, which has no indication of the presence of an AGN at any wavelength with the exception of the hard X-rays, where the AGN direct emission escapes the high column density ($N_H > 10^{24} \text{ cm}^{-2}$)

¹ In this paper we will not discuss powerful radio loud quasars, which have an infrared luminosity in the ULIRG range, mainly due to synchrotron emission of relativistic particles in the jet, but are not dominated by infrared radiation.

absorber at $E > 10 \text{ keV}$ (Vignati et al. 55), and the flat reflected emission, with a prominent iron $K\alpha$ emission line with equivalent width $EW > 1 \text{ keV}$ are observed in the 2-10 keV range.

(b) Extension to faint sources. The most powerful indicators of the presence of buried AGNs in ULIRGs have been proven to be the hard X-ray spectra, and ISO mid-IR spectra. In both cases a good signal-to-noise spectrum is needed in order to detect the AGN/starburst indicators: in the X-rays, a high S/N is required to disentangle the hard power law due to the AGN emission from the thermal component due to the starburst; in the mid-IR a high S/N is needed to have an accurate determination of the continuum and, consequently, a reliable measurement of the equivalent width of the PAH emission features. With current infrared detectors, the required spectral quality can be achieved only for a small number ($\sim 10 - 15$) of bright objects. A big improvement for the mid-IR analysis is expected thanks to the Spitzer Space Telescope, which will be able to provide high quality mid-IR spectra for several tens of ULIRGS, as first results have already confirmed (Armus et al. 3).

An interesting new way of studying ULIRGs has been proven to be L-band ($\sim 3 - 4 \mu\text{m}$) spectroscopy. Imanishi and collaborators (in particular, Imanishi & Dudley 2000) discussed the physics of the emission/absorption features in the 3-4 μm interval, and showed that low-resolution spectra of the brightest ULIRGs, obtained at 4 meter class telescopes, provide effective diagnostic elements in order to disentangle the AGN and starburst contributions to the observed emission. Recently, Imanishi, Dudley & Maloney (2005) applied this method to investigate the energy source in a sample of ~ 40 objects from the 1 Jy sample (Kim & Sanders 1998).

Risaliti et al. (2003) presented a high signal-to-noise L-band spectrum of the bright ULIRG IRAS 19254-7245 obtained with the instrument ISAAC at the Very Large Telescope (VLT) in Paranal, Chile. This high quality spectrum suggested that 8 meter class telescopes are able to provide good enough spectra for (a) a detailed study of the physical properties of bright ULIRGs, and (b) an analysis of relatively faint ULIRGs, for which other indicators are not available with the current instrumentation.

In this paper we present new L-band spectra of bright ULIRGs obtained with the instrument ISAAC at the VLT in Paranal, Chile, and we perform a complete analysis of the L-band diagnostics applied to a representative sample of ULIRGs, consisting of our new observations and previously available L-band spectra. In Section 2 we review the L-band spectral features useful in order to investigate the energy source in ULIRGs. In Section 3 we present our sample. In Section 4 we present the new L-band spectra. The physical analysis of each new spectrum is presented in Section 5. In Section 6 we present a detailed discussion of our results, and an analysis of the different indicators in a complete flux-limited sample, obtained merging our sample of southern sources with other spectra obtained by Imanishi and collaborators for northern ULIRGs. In particular: (1) we present new two-dimensional diagnostic diagrams where starburst and AGNs are completely separated (2) we discuss the physical properties of the dusty circumnuclear medium in ULIRGs hosting AGNs, showing that a different amount of hot dust absorption can explain the main differences among spectra of these sources; (3) we show that the amount

of hot dust can also explain the differences among starburst-dominated ULIRGs.

Our conclusions are summarized in Section 7. Through this paper we estimate luminosity distances using the WMAP concordance cosmology ($h_0 = 70$, $\Omega_m = 0.3$, $\Omega_\lambda = 0.7$, e.g. Spergel et al. 50

2 L-BAND DIAGNOSTICS FOR ULIRGS

Disentangling the contribution of heavily obscured AGNs and starbursts to the luminosity of ULIRGs is intrinsically complicated, because of the reprocessing, in both cases, of the primary optical/UV radiation into mid- and far-IR emission.

However, several physical differences between the two energy sources can have direct consequences on the observed reprocessed radiation in the infrared:

- The X-ray emission of an AGN, much stronger than that of a starburst (with respect to the bolometric emission) affects the gas and dust composition around the central source. For example, (a) highly ionized atomic species, requiring a strong ionizing X-ray continuum, are present only around AGNs, and (b) complex hydrocarbon dust grains can be present only around starbursts, while they cannot survive in the close vicinity of AGNs, since they are destroyed by the X-ray photons.
- An active nucleus is an extremely compact radiation source with respect to a starburst region. This implies that strong absorption effects in AGN spectra are easily obtained through compact and dense absorbers along the line of sight. The same effects are harder to obtain in starbursts, since the absorber should be large enough to cover the whole emitting region.
- The amount of high temperature (from a few 10^2 K to the sublimation temperature, $T_{sub} \sim 1,500$ K) dust is higher in AGNs than in starbursts. This affects the infrared spectral energy distribution, in particular in the near- and mid-IR.

In particular, the emission in the L-band is due to reprocessing of the primary radiation by hot dust (temperature in the range 100-1000 K), i.e. by material relatively close to the central source. As a consequence, the observed L-band spectra are heavily affected by the above physical differences.

Here we briefly review the main diagnostic features in ULIRGs, most of which are present in some of the spectra shown in Fig. 1. These indicators have been calibrated on objects for which the starburst/AGN classification is known from other, independent studies. However, several cases are known for which some of these diagnostic tools fail. We will discuss these cases, and possible improvements of the diagnostic techniques, in Section 6.

3.3 μ m emission feature. A strong, broad emission feature at a rest-frame wavelength $\lambda = 3.3\mu$ m is the most prominent non-continuum feature in the spectra of most ULIRGs. The origin of this emission feature is believed to be the reprocessing of UV radiation by polycyclic aromatic hydrocarbon (PAH) molecules. These complex organic

molecules (for a review on their structure and physical properties, see Allamandola, Tielens, & Barker 1) are responsible of several broad emission features in the mid-IR wavelength band, and have been extensively studied in ISO spectra of ULIRGs (e.g. G98).

The 3.3 μ m emission feature is particularly interesting in this context because it is an isolated feature, which can be easily disentangled from the continuum emission. This is not the case in many mid-IR ISO spectra, where the combination of broad emission features due to PAHs with broad absorption features due to dust makes the determination of the continuum level (and therefore of the equivalent width of the lines) extremely uncertain (one notable exception is the PAH emission feature at 6.2 μ m, as discussed in Fischer (12)).

Both theoretical and observational evidence suggests that the strength of the 3.3 μ m PAH feature is an indicator of the relative contribution of AGN and starburst to the emission of ULIRGs:

- Observationally, it is found that objects which are independently classified as starburst-dominated show a 3.3 μ m feature with an equivalent width $EW_{3.3} \sim 100$ nm or higher. This is true both at ULIRGs luminosities and for objects with luminosities of the order of $\sim 10^{11} L_\odot$ (Moorwood 34, Imanishi & Dudley 15). Objects known to be dominated by AGN emission show a weak or absent ($EW_{3.3} < 30$ nm) 3.3 μ m emission feature (Imanishi & Dudley 15). As we will discuss in more detail later, this is not a “perfect” indicator. However, the correlation is strong, and no exception is known at least in cases of extreme values (i.e. all known sources with $EW_{3.3} < 50$ nm or $EW_{3.3} > 100$ nm are dominated by AGN or starburst, respectively).
- From a physical point of view, two mechanisms are expected to be effective in decreasing the equivalent width of the 3.3 μ m line in AGNs: (a) the X-ray radiation can destroy the PAH molecules which are not shielded by a column density from a few 10^{22} to 10^{24} cm $^{-2}$ of gas, depending on the geometrical and physical conditions (Voit 56), and (b) the strong L-band continuum (much stronger than in starbursts due to the presence of a larger amount of hot dust) can dilute the 3.3 μ m emission from outer or gas-shielded starburst regions.

3.4 μ m absorption feature. A deep absorption feature is clearly present in the spectrum of several ULIRGs. The most prominent cases are IRAS 19254-7245S (Fig. 1, see Risaliti et al. 42 for details), UGC 5101 (Imanishi et al. 20) and IRAS 08572+3915 (Imanishi & Dudley 15), where the optical depth² at 3.4 μ m is $\tau_{3.4} \sim 0.8 - 1$. The origin of this feature is believed to be absorption by hydrocarbon dust grains, in particular by vibrational stretching levels of the C-H₂ and C-H₃ groups (Sandford et al. 47 and references therein, Pendleton & Allamandola 37). In the highest signal-to-noise detections, as the ones mentioned above, a detailed study of the chemistry of the absorbing dust is

² All the optical depth estimates presented in this paper are computed as the natural logarithmic ratio between the estimated continuum flux and the measured emission at the wavelength corresponding to the minimum of the absorption profile.

possible through the analysis of the substructure of the absorption profile (Risaliti et al. 42, Mason et al. 33).

The presence of the $3.4\mu\text{m}$ absorption feature is an indicator of a strong AGN contribution to the ULIRG emission. Again, the motivation has both a physical explanation and an observational confirmation:

- Observationally, all the above mentioned ULIRGs are independently known to host a powerful AGN. The other known cases among ULIRGs where this feature has been revealed (Imanishi & Dudley 15), even if with a smaller optical depth, are all classified as AGNs on the basis of independent classification at other wavelengths. Furthermore, L-band spectra of non-ULIRG obscured AGNs show strong $3.4\mu\text{m}$ absorption (Imanishi 16).

- Physically, in order to detect a high $3.4\mu\text{m}$ absorption optical depth, a high column density absorber in front of the primary source is required. Imanishi & Maloney (19) showed that dilution and saturation effects prevent the observed optical depth from being higher than ~ 0.2 in case the absorbing dust is spatially mixed with the energy sources. Therefore, in order to achieve high values of $\tau_{3.4}$, an external screen completely covering the radiation source is needed. Since the absorbing dust is expected to lie in gas clouds, we can estimate the amount of gas expected to be associated with the dust assuming a Galactic dust-to-gas ratio, and the extinction curve of Pendleton et al. (36). We find $N_H \sim 3 - 5 \times 10^{23} \tau_{3.4} \text{ cm}^{-2}$. The actual value could easily be more than an order of magnitude greater, given that the measured dust-to-gas ratio in AGNs is systematically lower than Galactic (Alonso-Herrero, Ward, & Kotilainen 2, Maccacaro, Perola, & Elvis 32, Maiolino et al. 31). Such high column densities are easily present around AGNs (\sim half AGNs in the local Universe are absorbed by column densities higher than 10^{24} cm^{-2} , Risaliti, Maiolino, & Salvati 40), while a complete covering of a starburst region would imply a huge amount of gas: assuming the linear dimension of a starburst region emitting $\sim 10^{12} L_\odot$ to be of the order of or greater than one kiloparsec, the required mass of gas would be $M_{\text{gas}} > 10^{11} \times (R/100 \text{ pc})^2 M_\odot$.

3.1 μm absorption feature. A broad absorption feature at $\sim 3.1 \mu\text{m}$ has been detected in several ULIRGs (Imanishi & Maloney 19). The origin of this feature is absorption by ice-covered dust grains. Analogously to the $3.4\mu\text{m}$ feature, it can be shown that optical depths $\tau_{3.1} > 0.3$ are not possible unless an external screen covering the source is present, if a fraction of 30% of dust grains covered by ice is assumed (as estimated for the nearby starburst M82, Imanishi & Maloney 2003). Then the same argument as above suggests that this is highly unlikely in starburst-dominated sources. This expectation is confirmed by the discovery of broad ice absorption in AGN-dominated ULIRGs (Imanishi & Maloney 19). However, the uncertainty on the possible profiles and widths of this absorption features makes it less straightforward than the previous indicators, especially in low signal-to-noise spectra. In particular, in many cases it is not possible to distinguish in AGN-dominated objects whether a concave spectrum in the $3-3.6\mu\text{m}$ region is due to a broad ice absorption feature, or to a change in spectral slope (in a $\lambda - f_\lambda$ plane) between the near-IR region (still dominated by the tail of the direct emission of the AGN accretion disc) and the mid-IR region (dominated by repro-

cessing of hot dust). In order to distinguish between these scenarios, a high signal-to-noise spectrum is required, in order to constrain the continuum slope using the feature-free $3.5-4 \mu\text{m}$ wavelength region. Alternatively a broader wavelength coverage, involving K-band and/or M-band spectra are needed. Moreover, a different (higher) fraction of dust grains covered by ice could increase the upper limit of $\tau_{3.1}$ in starbursts.

In the next Section we will separately discuss each case among our spectra where ice absorption could be present.

Continuum slope. The observed continuum slope in the L-band spectra of ULIRGs has a wide range, spanning from $\Gamma = \sim -2$ to $\Gamma \sim 3$ when fitted with a $f_\lambda = K\lambda^\Gamma$ model. Observations of known AGNs and starbursts suggest that positive Γ are an indication of AGN activity. The physical explanation of this trend is clear: a high Γ implies strong dust reddening of a compact source, and hence the presence of an AGN. As for the other indicators, we note that observations confirm the effectiveness of the continuum slope in extreme cases ($\Gamma > 2$ are always associated to AGNs), while objects with $\Gamma < 2$ (i. e. most of the ULIRGs observed so far) can be either AGNs or starbursts. We will go into further details on this point in Section 6.

Atomic emission lines. Atomic emission lines are in principle powerful diagnostics of the presence of an AGN. A broad atomic emission line, such as the $B\alpha$ line at $4.05 \mu\text{m}$, or a high ionization line such as the [SiIX] $\lambda 3.95 \mu\text{m}$ or the [MgVIII] $\lambda 3.028 \mu\text{m}$, are strong indicators of the presence of an AGN. These diagnostics have been successfully used on nearby Seyfert 2 Galaxies (Lutz et al. 29).

However, out of these three lines, by far the most intense expected in the (rest frame) L-band, two ($B\alpha$ and [SiIX]) are in all our objects out of the well calibrated $2.9-4.1 \mu\text{m}$ interval, due to the redshift effect, and the third one, [MgVIII] is in the poor atmospheric transmission interval (Fig. 1). Therefore, we will not use this diagnostics in this work.

3 THE BRIGHT ULIRGS SAMPLE

The sample chosen for L-band spectroscopic observations is the one of G98, consisting of 15 ULIRGs in the IRAS Bright Galaxy Sample (BGS, consisting of all the galaxies in the IRAS all sky survey with galactic latitude $\|b\| > 5^\circ$ and $60 \mu\text{m}$ flux density $S_{60} > 5.24 \text{ Jy}$, Sanders et al. 46), with two variations: one source (IRAS 23060+0305) has been dropped because it does not fulfill the flux requirement of the BGS, and two sources (IRAS 08572+3915 and IRAS 05189-2524) have been added, because they have $S_{60} > 5.24 \text{ Jy}$ (Table 1).

The luminosity criterion used to select ULIRGs is the standard one, i.e. $L_{\text{IR}} > 10^{12} L_\odot$, where L_{IR} is the total $8-1000\mu\text{m}$ luminosity, calculated using the IR flux equation of (45):

$$F_{\text{IR}} = 1.8 \times 10^{-11} (13.48S_{12} + 5.12S_{25} + 2.58S_{60} + S_{100}) \quad (1)$$

where F_{IR} is the total IR flux in units of $\text{erg s}^{-1} \text{ cm}^{-2}$, and $S_{12}, S_{25}, S_{60}, S_{100}$ are the flux densities in the four IRAS filters, in units of Jy.

One source, NGC 6240, has a slightly lower total infrared luminosity. However, it is included in our sample, as well as in that of G98, because all the morphological and physical properties appear to be typical of ULIRGs.

Two different considerations drove us in choosing this sample:

1. These are the IR brightest ULIRGs, therefore we expect to obtain the best possible quality for our L-band spectra. This is crucial at the present level of development of L-band diagnostics: as briefly discussed in the introduction, we still need to perform detailed studies of bright objects in order to better understand and calibrate the physical diagnostics, before applying this technique to a larger sample of fainter sources.
2. The sources in our sample are the best studied ULIRGs at other wavelengths. In particular, complete near-IR photometry and spectroscopy and ISO mid-IR spectroscopy is available, and in the X-rays we recently performed a complete X-ray spectroscopic study with *XMM-Newton* (Franceschini et al. 13, Braito et al. 5, Braito et al. 6). This will allow us (a) to investigate multi-wavelength indicators of the AGN/starburst contribution to the IR emission, and (b) to compare our results in the L-band with existing AGN/starburst classifications based on observations at other wavelengths.

Out of the 16 ULIRGs in our ULIRGs sample, we selected eight sources visible from Chile, and with no previous L-band spectroscopic observations. For six more sources (IRAS 05189-2524, MKN 231, MKN 273, UGC 5101, Arp 220, IRAS 08572+3915) in the sample 3-4 μ m spectra obtained at the 3.6m UKIRT and 3.0m IRTF telescopes have been published by Imanishi & Dudley (15) and Imanishi, Dudley, & Maloney (17). We will include their results in the discussion in Sect. 4.

For one source (NGC 6240) with an L-band spectrum available in the literature (Imanishi & Dudley 15), we recently obtained a new, higher quality spectrum with ISAAC. The results of this observations will be published elsewhere (Risaliti et al. 2005, in prep.). In the following we will refer to the results of this new observation.

For one source (IRAS 19254-7245S) we already published a detailed spectral analysis (Risaliti et al. 42). The results of this analysis will be included for completeness in tables and plots, but will not be further discussed.

We report in Tab. 1 the basic known photometric data of our sources.

4 OBSERVATIONS, AND DATA REDUCTION

The L-band spectra were obtained with the instrument ISAAC at the UT1 unit of the Very Large Telescope (VLT) on Cerro Paranal, Chile. All but two objects were observed during three nights on June 02-04, 2002. IRAS 20100-4156 and IRAS 22491-1808 were observed on July 30, 2004.

The sky conditions were photometric, with a seeing of the order of 1 arcsec in K (0.7 arcsec for IRAS 20100-4156). For all but one observations a 20x1 arcsec slit was used. For one source (IRAS 20100-4156) we used the 20x0.7 slit. We note that the seeing in the L band is typically better than in K. This is confirmed by the profile analysis made on our observations (see below for details), which show that

in all cases the fraction of slit loss is lower than 10%. 6 out of 8 sources (the exceptions being IRAS 20551-4250 and IRAS 22491-1808) are known mergers, with two distinct nuclei resolved in infrared imaging. For all these objects we chose the slit angle in order to obtain spectra for both nuclei. The angles were chosen based on 2MASS images, and on the short images taken before each spectral observation. In three cases (IRAS 12112+0305, IRAS 14348-1447, IRAS 23128-5919) we were able to obtain high quality spectra of both nuclei. In one object (IRAS 19254-7245) we obtained a high quality spectrum for the brightest nucleus, and a low S/N spectrum for the faintest one, enough for an estimate of the flux and continuum slope. In two objects (IRAS 17208-0014 and IRAS 20100-4156) we obtained a spectrum of the brightest nucleus only. Out of the two single nucleus sources, we obtained a high quality spectrum of IRAS 20551-4250, while IRAS 22491-1808 was not detected.

The on-source time varies from one hour for the brightest objects to ~ 3 hours for the faintest. The observations were performed with the low resolution grating (LR) in the L band, with a coverage of the $\sim 2.9 - 4.1 \mu\text{m}$ wavelength band with a resolution $\lambda/\Delta\lambda \sim 360$.

The main data regarding the observations are listed in Table 2.

In order to avoid saturation due to the high background (~ 3.9 mag per arcsec 2 in L-band) all the spectra were taken in chopping mode, with single exposures of 0.56 s. The spectra were then aligned and merged into a single image. We performed a standard data reduction, consisting of flat-fielding, background subtraction, and spectra extraction, using the IRAF 2.11 package.

For each object we also acquired the spectrum of a standard star immediately before or after the target observation. The star was chosen in order to have the same airmass as the target, within 0.1, and with an L magnitude between 4 and 6. This allowed us to obtain high quality spectra with 2 minute long observations.

Corrections for sky absorption and instrumental response were obtained from the standard stars spectra. All the standards are B stars, therefore we assumed a pure Raleigh-Jeans intrinsic spectrum in the L-band.

In order to facilitate the background subtraction, the observations were performed using a mosaic consisting in a shift of the slit by 20 arcsec up and down along the chosen direction. However, the instrumental response is not constant along the slit direction (this effect is mostly removed by the flat-fielding; however, given the high level of noise, residual differences would strongly affect the final result). We compensated for this effect performing a separate reduction for each of the three spectra relative to the three different positions along the slit. The results before the divisions by the three standard star spectra (obtained in the same way) were in general quite different one from the other, both in absolute flux and in spectral shape. However, after the division by the stars, the three spectra of all sources overlapped within the errors. This gives us an important self-consistency check for our spectral reduction procedure.

In order to obtain a precise absolute calibration, we took into account aperture effects by analyzing the profiles of both the targets and the standard stars along the slit. We assumed a Gaussian profile and we estimated the fraction of flux inside the slit assuming a perfect centering. We estimate

Name	z	S_{12}^a	S_{25}^a	S_{60}^a	S_{100}^a	L_{IR}^b	J^c	H^c	K^c	$S_{5.9}^d$	$S_{7.7}^d$
IRAS 12112+0305SW	0.072	0.06	0.29	5	5.8	1.1	—	—	14.3	5.9	7.7
IRAS 12112+0305NE	”	0.04	0.21	3.5	4.2	0.8	—	—	14.5	”	”
IRAS 14348-1447S	0.082	0.07	0.33	4.5	4.7	1.3	15.6	14.7	13.7	1.3	1.9
IRAS 14348-1447N	”	0.03	0.17	2.4	2.4	0.7	16.1	15.1	14.3	”	”
IRAS 17208-0014A	0.043	0.2	1.7	31.1	34.9	2.3	14.0	12.9	12.4	3.2	4.9
IRAS 19254-7245S	0.062	0.19	1.15	5.3	5.6	1.1	14.0	12.7	11.7	7.0	9.5
IRAS 19254-7245N	”	0.01	0.05	0.2	0.2	0.2					
IRAS 20100-4156	0.130	0.1	0.3	5.2	5.2	3.6	15.0	14.3	13.7	1.4	2.1
IRAS 20551-4250	0.043	0.3	1.9	12.8	10.0	1.1	13.4	12.2	12.2	4.5	7.0
IRAS 22491-1808	0.078	0.1	0.6	5.4	4.5	1.5	14.7	14.0	13.6	1.5	4.4
IRAS 23128-5919N	0.044	0.05	0.3	2.9	2.7	0.2	14.7	13.7	13.3	4.2	6.4
IRAS 23128-5919S	”	0.15	1.3	7.9	7.3	7.0	14.3	13.4	12.6	”	”

Table 1. Photometric NIR to FIR data for our sources. In five cases we report NIR photometry for two components of the sources. These are the cases where we were able to disentangle the two components in our L-band observations. For these objects we scale the total IRAS fluxes according to the K magnitudes of the single nuclei. Notes: ^a: flux density in the IRAS filters, in units of Jy; ^b: Total infrared luminosity in units of $10^{12} L_{\odot}$, estimated from Eq. 1 and assuming the concordance cosmology ($H_0, \Omega_m, \Omega_{\Lambda}$) = (70, 0.3, 0.7), Spergel et al. 50). ^c: Infrared magnitudes from Duc, Mirabel, & Maza (9), except for the K magnitudes of the two nuclei of IRAS 12112+0305, which are from Kim, Veilleux, & Sanders (25); ^d: Mid-IR flux densities obtained with ISO, from Rigopoulou et al. (39).

Source	Observation Date	T ^a	Slit width	Pos. Angle ^b	Standard Star	Type	L ^c
IRAS 12112+0305	2002-06-02	180	1"	35	Hip 076126	B3V	5.92
IRAS 14348-1447	2002-06-03	180	1"	25	Hip 065630	B3IV	6.52
IRAS 17208-0014	2002-06-02	60	1"	0	Hip 076126	B3V	5.92
IRAS 19254-7245/1	2002-06-02	60	1"	170	Hip 076126	B3V	5.92
IRAS 19254-7245/2	2002-06-03	60	1"	170	Hip 000183	B4V	5.42
IRAS 20100-4156	2004-07-30	90	0.7"	0	Hip 011407	B5IV	4.65
IRAS 20551-4250	2002-06-02	60	1"	0	Hip 076126	B3V	5.92
IRAS 22491-1808	2002-06-02	60	1"	0	Hip 076126	B3V	5.92
IRAS 23128-5919/1	2002-06-02	60	1"	0	Hip 038593	B2V	5.98
IRAS 23128-5919/2	2002-06-03	60	1"	0	Hip 000183	B4V	5.42

Table 2. Observation log of our ISAAC program. 2 sources were observed twice. Notes: ^a: observing time in minutes. ^b: Slit position angle, with respect to the north-south inclination. The angle increases in counter-clockwise direction, starting from the north. ^c: L magnitude of the standard star.

this procedure to have an error of the order of $\sim 10 - 15\%$ or better. In three cases (Table 2) this is confirmed by the comparison of the spectra obtained in two different nights, and corrected with two different standard stars: the final calibrated spectra are always consistent within the errors. A further consistency check is provided by the comparison with the magnitudes at longer wavelengths (when available from ISO observations), which show a good agreement with our results.

For each source the final spectrum, obtained (a) merging the three single spectra relative to the three slit positions, and (b), when two or more observations were present, merging the final calibrated spectra, was rebinned in order to have a statistical significance of each bin of at least 2σ .

The error bars were estimated from the Poissonian noise in the sky counts, which are by far the dominant source of noise (for ease of comparison, our brightest source has a magnitude $L \sim 11$, i.e. a ~ 600 times lower flux than the sky background in the same extraction region).

The final L-band spectra of our sources are shown in Fig. 1.

5 DATA ANALYSIS

As a first step for the interpretation of the L-band spectra of our sample of ULIRGs, we fitted the “feature-free” continuum with a single power law. The chosen wavelength interval is the 3.4-4 μm (rest frame) for all sources except IRAS 19254-7245S and IRAS 20551-4250, where we took into account the conspicuous absorption features at $\sim 3.4 \mu\text{m}$. The best fit power laws are plotted in Fig. 1, in order to better analyze the absorption and emission features.

As a second step, we fitted the whole spectra in order to quantitatively measure the relevant parameter of the major spectral features. The best fit model consists of a power law, an emission line at rest frame wavelength $\lambda_{rest} \sim 3.3 \mu\text{m}$, and when needed an absorption feature (with Gaussian profile) at $\lambda_{rest} \sim 3.4 \mu\text{m}$ (hydrocarbon dust grain absorption) and one at $\lambda_{rest} \sim 3.1 \mu\text{m}$ (water ice absorption). The results of the spectral fits are shown in Tab. 3.

Here we briefly discuss the spectrum of each source, estimating the AGN/starburst contribution and comparing our results with those obtained through the observations at other wavelengths. In particular we refer to G98 for ISO mid-IR spectroscopy, and to Franceschini et al. (13) for

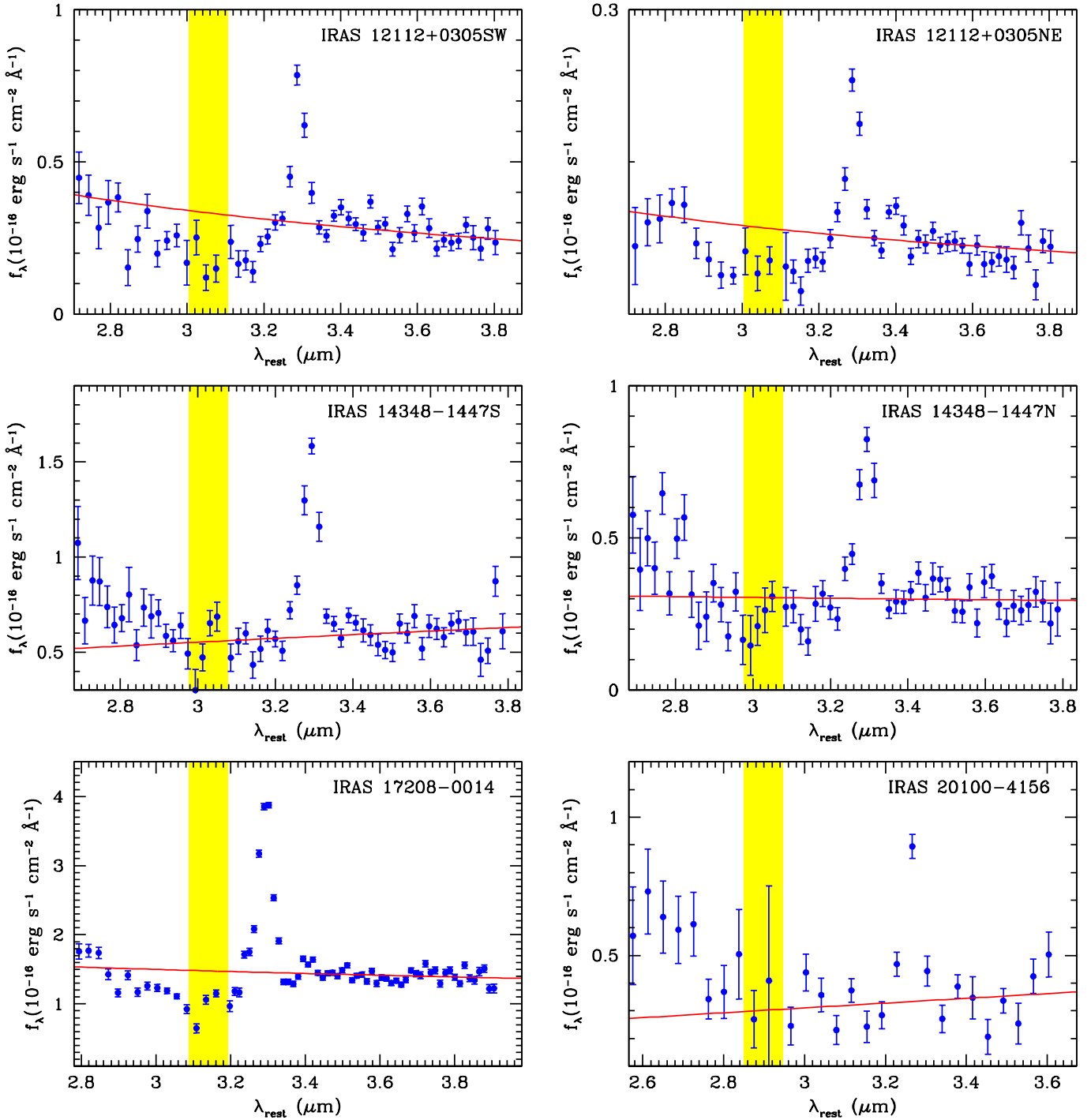


Figure 1. Flux-calibrated L-band spectra of our sample of ULIRGs. Wavelengths are in the rest frame. The shaded vertical band shows the spectral region with bad atmospheric transmission. In each spectrum, the continuous line represents a power law model fitted on the spectral region red-ward of the broad emission feature at $3.3\mu\text{m}$ (i.e. at $\sim\lambda > 3.4\mu\text{m}$ in the rest frame). Exceptions are IRAS 19254-7245S and IRAS 20551-4250, where the two obvious absorption features at $\sim 3.4 - 3.5\mu\text{m}$ were also excluded from the fitting region.

XMM-Newton X-ray spectroscopy.

IRAS 12112+0305. The two nuclei in this source have similar L-band spectra. In both cases the high equivalent width of the $3.3\mu\text{m}$ line, the absence of $3.4\mu\text{m}$ absorption and the flat spectrum suggest a starburst origin

for their infrared luminosity. This is in agreement with the classification at other wavelengths:

- in the optical, the $[\text{OIII}]/\text{H}\beta$ ratio, and the low flux of $[\text{NII}]\lambda 6583\text{\AA}$, $[\text{SII}]\lambda 6716\text{\AA}$ and $[\text{OI}]\lambda 6300\text{\AA}$ with respect to $\text{H}\alpha$, suggest a LINER classification (Veilleux, Kim, & Sanders 53).

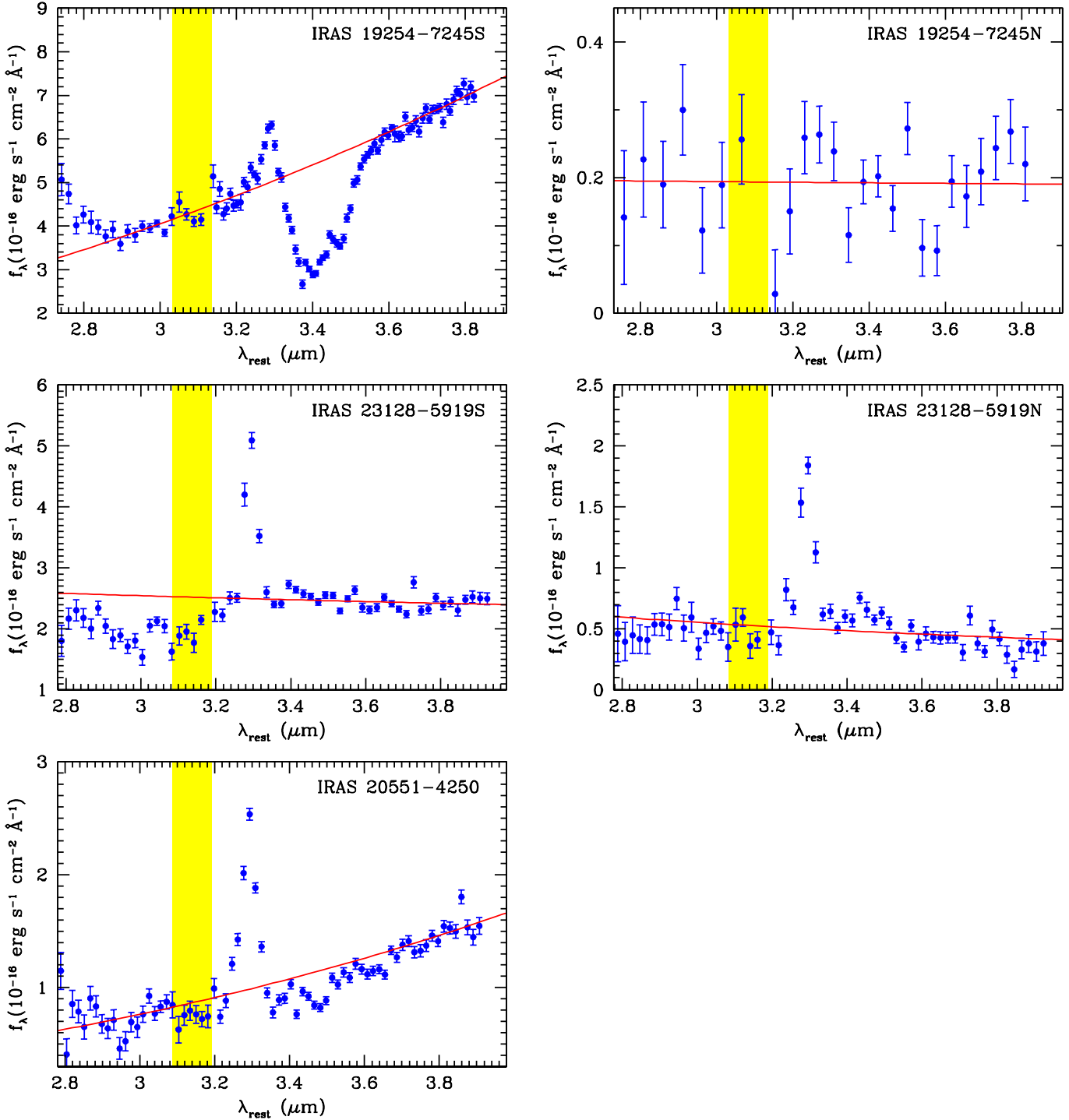


Figure 1. - Continued.

- in the mid-IR the high equivalent width of the $7.7 \mu\text{m}$ PAH emission feature suggests a pure starburst classification.
- in the hard X-rays no indication of AGN activity is found.

IRAS 14348-1447. The L-band spectrum of both nuclei is dominated by a high equivalent width $3.3 \mu\text{m}$ emission feature ($\text{EW} > 100 \text{ nm}$). The continuum is \sim flat in both cases, with an uncertainty in the brightest nucleus (S) due to a possible presence of a moderate ($\tau \sim 0.1 - 0.2$)

ice absorption. If we allow for ice absorption, the best fit continuum slope is $\Gamma \sim -0.2$, while without ice absorption $\Gamma \sim 0.5$. The values in Tab. 3 refer to the fit to a power law+emission line model, without absorption features. This model provides a good representation of the continuum, with a small excess in the $2.9-3.1 \mu\text{m}$, which could be due to the tail of the K-band emission coming from a broader region than the L-band emission. The starburst classification is confirmed by ISO mid-IR spectroscopy and

name	Γ^a	$EW_{3.3}^b$	$\tau_{3.1}^c$	$\tau_{3.4}^d$	L^e	$\log[(\lambda l_\lambda)_{3.5}/L_\odot]^f$
IRAS 12112+0305SW	-0.64 \pm 0.3	78 \pm 21	0.5 \pm 0.1	—	13.4	9.5
IRAS 12112+0305NE	-1.4 \pm 0.5	97 \pm 34	0.5 \pm 0.1	—	13.8	9.3
IRAS 14348-1447S	0.55 \pm 0.3	98 \pm 23	—	—	12.7	9.9
IRAS 14348-1447N	-0.13 \pm 0.6	100 \pm 37	—	—	13.5	9.6
IRAS 17208-0014	-0.32 \pm 0.1	83 \pm 5	0.4 \pm 0.05	—	11.7	9.7
IRAS 19254-7245S	2.30 \pm 0.03	26 \pm 3	—	0.8 \pm 0.05	10.3	10.6
IRAS 19254-7245N	0.1 \pm 1.2	—	—	—	13.9	9.2
IRAS 20100-4156	0.85 \pm 0.7	92 \pm 41	—	—	13.3	10.0
IRAS 20551-4250	2.75 \pm 0.13	72 \pm 9	—	0.3 \pm 0.1	12.0	9.6
IRAS 23128-5919S	-0.2 \pm 0.1	43 \pm 5	0.45 \pm 0.05	—	11.1	10.0
IRAS 23128-5919N	-1.05 \pm 0.2	130 \pm 22	—	—	12.7	9.4

Table 3. Spectral analysis results. a : Slope of the continuum power law, defined as $f_\lambda \propto \lambda^\Gamma$. b : Equivalent width of the 3.3 μm emission feature, in units of nm. c : Optical depth of the 3.1 μm ice absorption feature. d : Optical depth of the 3.4 μm hydrocarbon absorption feature. e : L magnitude. f : luminosity λl_λ at 3.5 μm , in log of bolometric solar luminosity.

X-ray spectroscopy.

IRAS 17208-0014. The L-band spectrum is dominated by a strong PAH 3.3 μm emission feature. The continuum slope $\Gamma \sim 0.3$ is indicative of a starburst origin of the L-band emission. An ice absorption feature at 3.1 μm is clearly detected. A single Gaussian absorption component is significant at a 5 σ statistical level. This, together with IRAS 23128-5919S, is the best constrained ice absorption feature among the sources in our sample, thanks to the high S/N spectrum which allows a precise continuum determination. The estimated optical depth is $\tau_{3.1} = 0.4 \pm 0.05$. In the mid-IR and X-rays IRAS 17208-0014 appears dominated by starburst activity.

IRAS 19254-7245. The high quality spectrum of the southern nucleus show both a 3.3 μm emission feature with an equivalent width ($\text{EW} \sim 25$ nm), and two clear AGN features, i.e. a steep continuum ($\Gamma = 2.3$) and a strong absorption at 3.4 μm ($\tau = 0.8$). The substructures of the absorption profile can be used to constrain the chemical composition of the absorbing dust. A detailed analysis of this spectrum is presented in Risaliti et al. (42). The northern nucleus is extremely faint, and a detailed spectral analysis is not possible. The continuum is flat, and no spectral feature is present. The low S/N prevents us from performing any further analysis. A detailed study of the multiwavelength spectral energy distribution led to the conclusion that the infrared emission of this nucleus is due to an inactive galactic component (4).

IRAS 20100-4156. Only the brightest nucleus of this source is detected. The spectrum (the lowest S/N among the primary nuclei in our sources) is dominated by the 3.3 μm emission line, suggesting a starburst origin of the L-band emission. The continuum slope is quite uncertain, due to the low S/N. An argument similar to that for IRAS 12112-0305NE can be applied: the continuum can be fitted (a) by a flat power law, with a residual excess at 2.9-3 μm , or (b) by a steeper ($\Gamma \sim -0.5$) continuum plus an ice absorption feature with $\tau_{3.1} \sim 0.5$. In both interpretations, no clear indication of the presence of an AGN is found, even if we cannot rule out a possible minor AGN contribution, due to the low statistics available.

The mid-IR spectrum of this source suggests a starburst classification. In the X-rays, no clear indication of an AGN is found, however the location of this source in the X-ray diagnostic diagrams of Franceschini et al. (13) is between the typical starbursts and AGNs positions, suggesting a possible contribution of an AGN.

IRAS 20551-4250. The high quality spectrum of this source is the most puzzling in our sample. A strong 3.3 μm emission feature ($\text{EW}=70$ nm) suggests a dominance of the starburst contribution. However, a steep and inverted continuum slope ($\Gamma \sim 2.7$) and the presence of a 3.4 μm absorption feature ($\tau_{3.4} \sim 0.3$) points to the presence of an AGN dominating the continuum emission. This is a clear example where the simple classification, based on the spectral diagnostics described in the previous section, fails. We will discuss this source further in Section 6, where an improvement of the above indicators will be discussed. The mid-IR spectrum of IRAS 20551-4250 shows clear indications of the presence of an AGN. Similarly, the X-spectrum is typical of a heavily absorbed AGN-dominated source. The presence of the AGN was also revealed by the analysis of the polarized optical spectrum (38).

Risaliti et al. (42) and Mason et al. (33) showed that a detailed investigation of the chemistry of the dust grains responsible of the 3.4 μm absorption is possible, based on the analysis of the substructure of the 3.4 μm absorption feature. Such analysis on the only other source of our sample showing the 3.4 μm absorption feature, IRAS 19254-7245, led to the conclusion that the dust composition in that source is remarkably similar to that observed in Galactic stellar sources.

The continuum-subtracted spectrum of IRAS 20551-4250 in the 3.3-3.8 μm range is plotted in Fig. 2. A hydrocarbon dust absorption feature is clearly visible in Fig. 2, and confirmed by the fit with a single Gaussian absorption component, which is significant at $> 3 \sigma$. A detailed analysis of the chemical composition of the absorbing dust (analogous to that done in R03 and Mason et al. (33) is not possible here, because of the low S/N and the low optical depth ($\tau \sim 0.3$ when fitted with a single Gaussian profile). However, from a qualitative analysis of Fig. 2 we can tentatively note a stronger absorption dip at $\sim 3.5 \mu\text{m}$ with respect to the Galactic source IRS7

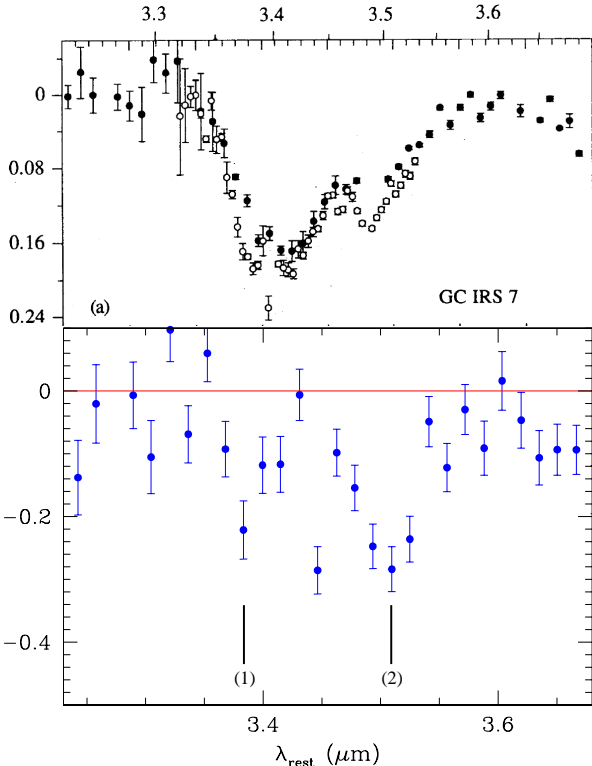


Figure 2. Continuum-subtracted spectrum of IRAS 20551-4250 in the 3.3-3.8 μm wavelength range, compared with the spectrum of the Galactic center source IRS 7 (36). The complex structure of the hydrocarbon dust absorption feature is clearly visible. The first dip is due to vibrational transitions of pure aliphatic hydrocarbon molecules; the second dip is due to the same transitions in hydrocarbon molecules where electronegative group, such as $-\text{NO}_2$ or $-\text{OH}$, are present.

(Pendleton et al. 36) and IRAS 19254-7245 (Risaliti et al. 42). This would imply that the hydrocarbon molecules responsible for absorption in this spectral region are richer than in the other two sources of electronegative groups such as $-\text{NO}_2$ and $-\text{OH}$.

IRAS 23128-1808. The southern nucleus has a flat continuum, with a moderate equivalent width 3.3 μm emission ($\text{EW}_{3.3} = 43 \pm 5$, well below the typical value for starbursts). A strong ice absorption ($\tau_{3.1} = 0.45$) is clearly detected. The relatively low EW of the 3.3 μm suggests the presence of an AGN. The 3.1 μm absorption feature also suggests the presence of a compact source. In this case, the good continuum determination leaves no doubts on the interpretation of the 2.9-3.3 μm spectrum, since the alternative scenario of an inverted continuum and a 2.9-3 μm excess is ruled out by the data. The northern nucleus has a typical starburst spectrum with a steep continuum and a strong 3.3 μm emission line ($\text{EW} \sim 130$ nm). No AGN indication is found in mid-IR spectra, while the hard X-ray spectrum clearly reveals the presence of an AGN. This source is therefore a case where the L-band analysis proves to be more effective than ISO spectroscopy in revealing the presence of an active nucleus as the origin of the infrared emission.

Summary. We analyzed the L-band spectra of 7 ULIRGs, 6 of which consisting of two distinct nuclei. All the single nuclei were detected except the faintest one in IRAS 20100-4156. The main results can be summarized as follows:

- A direct evidence for the presence of an AGN (equivalent width of the 3.3 μm emission feature $\text{EW}_{3.3} < 50$ nm, and/or steep and inverted continuum with $\Gamma < -1$, and/or 3.4 μm absorption feature) has been detected in three cases (IRAS 19254-7245, IRAS 20551-4250, IRAS 23128-5919). All these three sources have been classified as AGNs in our *XMM-Newton* X-ray survey of ULIRGs (Franceschini et al. 13).
- In two of the above cases the AGN indicators are not in agreement: the continuum of IRAS 23128-5919S is not inverted, and $\text{EW}_{3.3}$ of IRAS 20551-4250 is typical of a pure starburst.
- In two more nuclei (IRAS 12112+0305SW and IRAS 17208-0014) the detection of a strong ice absorption feature at 3.1 μm is unambiguous. No other AGN indication is present in these two sources either in the L-band or at other wavelengths.
- A possible absorption feature in the 3.0-3.2 μm range is detected in four more nuclei (IRAS 12112+0305NE, IRAS 14348-1447S and N, IRAS 20100-4156). In these cases, the interpretation as ice 3.1 μm absorption is not unique. An alternative fit can be obtained with a flatter or inverted continuum, plus a 2.9-3.0 μm excess due to the tail of the near-IR emission of the host galaxy.

6 ANALYSIS OF A COMPLETE SAMPLE

The L-band spectra described above represent a significant step forward in our study of ULIRGs, for three main reasons:

- **High quality.** The high signal-to-noise allowed a precise determination of the parameters of the main spectral features in most spectra (Tab. 3).
- **Completeness.** Our small sample consists of the sources of the G98 sample visible from Chile at the time of the observations. Since the G98 sample is made by the brightest known ULIRGs, and we did not introduce any physical bias, our sources can be considered as representative of ULIRGs in the local Universe. Moreover, combining our results with those of Imanishi & Dudley (15) and (17) we have good quality L-band spectroscopy of 13 objects out of the 15 of the G98 sample. This almost complete sample can be used to obtain statistical estimates on the average properties of ULIRGs in the local Universe.
- **Broad spectral coverage.** The availability of observations at other wavelengths (optical, near-IR, mid-IR, X-rays) allows a direct comparison of our results with those obtained with other, independent spectral diagnostics. This is fundamental in two respects: (a) it allows a precise calibration of the L-band starburst/AGN indicators, and (b) a study of the complete spectral energy distribution of these sources is possible.

We will use these properties in order to discuss three fundamental issues about the nature of ULIRGs: (1) Are L-band indicators capable to disentangle the AGN and starburst contributions in all cases? And is L-band spectroscopy

Name	Γ^a	$EW_{3.3}^b$	$\tau_{3.4}^c$	$\log[(\lambda l_\lambda)_{3.5}/L_\odot]^d$	$\log L_{3.3}/L_\odot^e$	L_{IR}^f
UGC 5101	5±0.5	35±10	0.65±0.05	10.1	8.1	0.95
Arp 220	0.05±0.05	82±10	—	9.3	7.6	1.5
NGC 6240	-0.1±0.1	50±10	—	9.9	8.1	0.72
MKN 273	0.7±0.2	35±5	—	10.1	8.0	1.4
MKN 231	-0.5±0.1	2±0.05	< 0.02	11.5	8.2	3.4
IRAS 08572+3915	2.4±0.2	< 2	0.9±0.05	10.7	< 7.3	1.4
IRAS 05189-2524	0.1±0.1	4±1	0.04±0.01	10.9	8.1	1.5
NGC 253	0.0±0.2	120±10	—	7.4	5.8	0.014
IC 694	0.3±0.2	150±10	—	9.0	7.5	0.74
MKN 463	-0.2±0.2	< 0.8	0.12±0.01	11.3	< 7.6	0.58
IRAS 20460+1925	-0.3±0.2	< 0.5	—	11.7	< 7.9	3.3
IRAS 23060+0505	0.1±0.2	< 1	—	11.8	< 8.3	2.8

Table 4. Spectral parameters of the ULIRGs in the complete sample and of five control sources (in the last five lines). Data are from (15) except for UGC 5101 (Imanishi, Dudley, & Maloney 17), MKN 463 (Imanishi 18), and NGC 6240 (Risaliti et al. 2005). ^a: Spectral index of a power law fitting the 3.4-4.0 μm continuum. The values are inferred from a visual inspection of the published spectra. ^b: Equivalent width of the 3.3 μm emission feature. The errors are conservative estimates based on visual inspection, except for the source UGC 5101, for which the error is reported in (17). ^c: optical depth of the 3.4 μm absorption feature. ^d: Log of the λf_λ luminosity at 3.5 μm , in units of L_\odot . ^e: Logarithmic ratio between the luminosity of the 3.3 μm emission feature and the total IR luminosity. ^f: Total infrared luminosity in units of $10^{12} L_\odot$, estimated from IRAS fluxes according to Eq. 1.

effective in finding AGNs in ULIRGs, with respect to indicators at other wavelengths? (2) How common are AGNs among ULIRGs? (3) When an AGN is present, is it possible to estimate the relative contribution of the AGN and starburst components to the total luminosity?

In the following, when the sample completeness is required (as, for example, in estimating the fraction of ULIRGs hosting an AGN) we will use the complete sample described above. When completeness is not required, we will add to the above sample a few more sources, with luminosity in the ULIRG range, or slightly lower, well known to be either starburst- or AGN-dominated in the L-band. This will increase the statistics and provide safer references for our interpretation. The relevant properties of these “control sources” are listed in Table 4.

6.1 L-band Diagnostic Diagrams

All the sources in our sample are well studied at other wavelengths, and the starburst/AGN contribution to their luminosity has been deeply investigated. The availability of an independent classification is useful to calibrate our L-band indicators, and to check their effectiveness. In Tab. 5 we report the indications about the presence of an AGN from several L-band indicators, and from studies at other wavelengths.

The most important result emerging from the analysis of Tab. 3-5 is that in *all cases* where one indicator suggests the presence of an AGN (i.e. low $EW_{3.3}$, $\tau_{3.4} > 0$, or $\Gamma > 1$) this is confirmed by independent classification.

As a further step in the search for empirical indicators of the AGN/starburst presence in ULIRGs, we combined the main AGN/SB indicators in order to study the possible correlations among them.

a) We plotted our sources in a $EW_{3.3} - \Gamma$ plane (Fig. 3a). This plot shows that an almost 100% effective L-band classification is possible: AGNs and starbursts lie in two different regions in the $EW_{3.3} - \Gamma$ plane.

b) Fig. 3b shows that the same clear division is obtained

by plotting $EW_{3.3}$ versus the R_L^{corr} , defined as the logarithmic L-band to total infrared ratio, corrected for L-band continuum absorption. In order to estimate the absorption in the L-band, we made use of the relation $A_L \sim 12\tau_{3.4}$ (Pendleton et al. 36).

These two results show the power of L-band spectroscopy in detecting AGNs among ULIRGs.

It is worth noting that the importance of the above analysis is related to the possibility of a large extension of the present work.

If we only limit our study to the sample analyzed here, our results are only a confirmation of the conclusions already obtained through studies at other wavelengths, in particular X-rays. However, the relatively low signal to noise of the X-ray spectra of these objects (which are the brightest known ULIRGs) obtained with *Chandra* (Ptak et al. 35) and *XMM-Newton* (Franceschini et al. 13) clearly indicates that it is not possible to extend the X-ray analysis to fainter objects. On the contrary, the quality of our spectra show that it is possible to obtain a rough estimate of the continuum slope and the 3.3 μm PAH feature equivalent width for a source as faint as $L \sim 14$.

Considering the average L-band / FIR ratio (Fig. 3), at least half of the sources in the IRAS 1 Jy sample of ULIRGs (Kim & Sanders 24) are expected to be brighter than this limit. This implies that our method, that has been calibrated here thanks to the availability of multi-wavelength observations of our bright sources, is capable to provide a statistical analysis on the presence of AGNs in a representative sample of 70 objects with redshift $z < 0.15$. (a first sample of ~ 40 sources observed with Subaru (Imanishi, Dudley & Maloney 2005) is already available for this purpose, and more sources are scheduled for observation with ISAAC at the VLT in the next few months. This will be the subject of a future paper).

Even more optimistic predictions are possible if we take into account that adaptive optics instruments are now available for L-band spectroscopy, like the NAOS-CONICA at

Name	L-band			Optical	Ref	Mid-IR	Ref	X-rays	Ref	
	$EW_{3.3}$	Γ	$\tau_{3.4}$							
UGC 5101	AGN	AGN	AGN	1	SB	4	SB	8	AGN	9
Arp 220	SB	SB	SB	2	SB	4	SB	8	AGN/SB	10
NGC 6240	AGN	AGN	SB	13	SB	5	SB	8	AGN	11
MKN 273	AGN	AGN	SB	2	AGN	4	AGN	8	AGN	12
MKN 231	AGN	SB	AGN	2	AGN	6	AGN	8	AGN	12
IRAS 05189-2524	AGN	SB	SB	2	AGN	14	AGN	4	AGN	15
IRAS 08572+3915	AGN	AGN	AGN	2	SB	4	AGN	8	AGN	6
IRAS 12112+0305	SB	SB	SB	3	SB	4	SB	8	SB	12
IRAS 14348-1447	SB	SB	SB	3	SB	4	SB	8	SB	12
IRAS 17208-0014	SB	SB	SB	3	SB	5	SB	8	SB	12
IRAS 19254-7245	AGN	AGN	AGN	3	AGN	7	SB	8	AGN	12
IRAS 20100-4156	SB	SB	SB	3	SB	7	SB	8	AGN/SB	12
IRAS 20551-4250	AGN	AGN	AGN	3	SB	7	SB	8	AGN	12
IRAS 23128-5919	AGN	SB	SB	3	SB	4	SB	8	AGN	12

Table 5. Detection of an AGN (either dominant or weak compared with the starburst component) in the complete sample of ULIRGs, according to several L-band, optical, mid-IR and X-ray spectroscopy. References: 1: Imanishi, Dudley, & Maloney 17; 2: Imanishi & Dudley 15; 3: This work; 4: Veilleux, Kim, & Sanders 53; 5: Veilleux et al. 52; 6: Sanders et al. 44; 7: Duc, Mirabel, & Maza 9; 8: Lutz, Veilleux, & Genzel 28; 9: Imanishi et al. 20; 10: Iwasawa et al. 23; 11: Vignati et al. 55; 12: Franceschini et al. 13; 13: Risaliti et al. 43; 14: Laureijs et al. 26; 15: Severgnini et al. 49

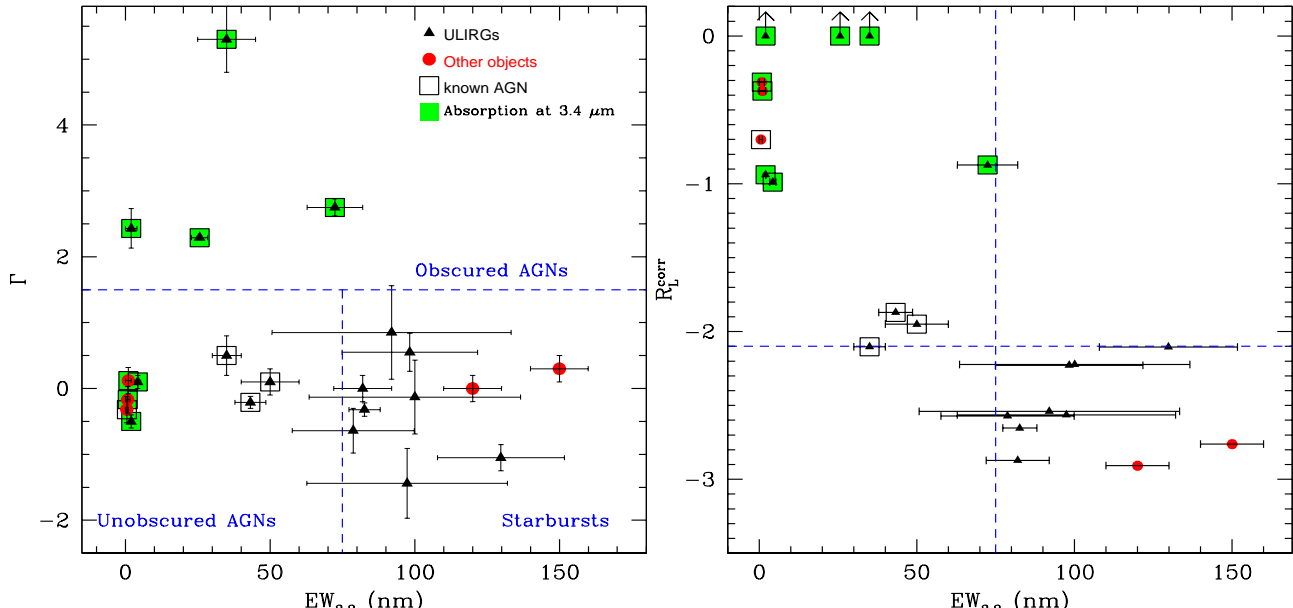


Figure 3. Left: $\Gamma - EW_{3.3}$ plot for our sample of ULIRGs and control sources. Right: equivalent width of the $3.3 \mu\text{m}$ emission feature versus the logarithmic ratio R_L^{corr} between absorption corrected L-band continuum luminosity and total IR luminosity. Errors on R_L^{corr} are of the order of, or smaller than, the size of the points. The straight lines are empirical divisions between AGNs and starbursts.

VLT. Since the noise in L-band observations of our sources is completely dominated by the thermal background ($\sim 3.9 \text{ mag/arcsec}^2$) a factor 10 smaller slit aperture (0.1 arcsec instead of 1 arcsec) would imply a significant increase of the signal-to-noise, even when efficiency losses due to the adaptive system are taken into account.

6.2 Physical properties of the nuclei of ULIRGs

In the previous Section we discussed the effectiveness of the L-band indicators in detecting AGNs in ULIRGs. Even if we demonstrated that such indicators are indeed effective from a practical point of view, it is not obvious to find a relation

between the variety of the observed L-band properties of our sample of ULIRGs and their physical properties.

Here we want to investigate this fundamental issue, through a physical interpretation of the indicators discussed above and of the results of observations at other wavelengths.

Among AGNs, an apparent spread in spectral properties suggests a high heterogeneity in the physical properties of the central emitting regions. However, two further indications suggest a simple physical interpretation: 1) The correlation between the continuum slope, Γ , and the optical depth at $3.4 \mu\text{m}$, $\tau_{3.4}$ is shown in Fig. 4. The sources with $\Gamma > 1$ are those with a high $3.4 \mu\text{m}$ absorption

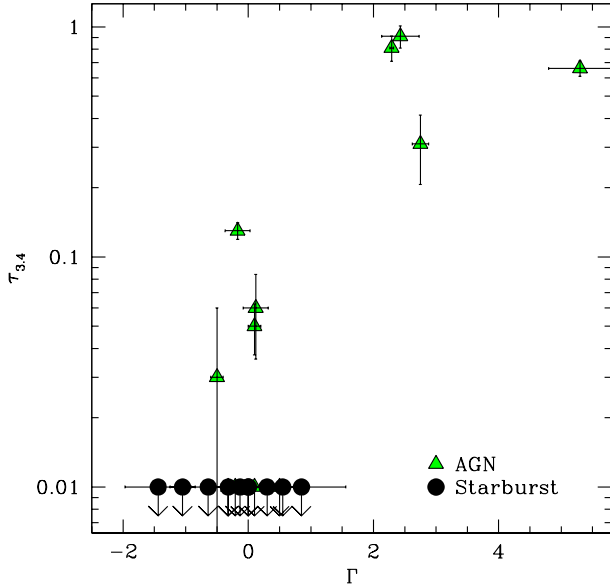


Figure 4. $3.4 \mu\text{m}$ absorption versus continuum slope for our sample of ULIRGs and control sources. Typical errors on $\tau_{3.4}$ are of the order of 10%.

($\tau_{3.4} > 0.3$). All the other sources are clustered around the ($\Gamma \sim 0, EW_{3.3} \sim 0$) point in Fig. 3a. 2) All AGNs in the ($\Gamma \sim 0, EW_{3.3} \sim 0$) group (Fig. 3) are not heavily absorbed in the X-rays (column densities in the range $22 < \log N_H < 23.5$), while all the high Γ , high $\tau_{3.4}$ objects have $\log N_H > 24$. Assuming a Galactic dust to gas ratio, $\log N_H \sim 23$ implies $A_L \sim 3$. If the dust to gas ratio is lower than Galactic, as suggested in all cases where a direct measurement is possible (Maiolino et al. 31), the absorption in the L-band is even smaller.

Combining the above indications, a physical interpretation clearly emerges:

- ($\Gamma \sim 0, EW_{3.3} \sim 0$) AGNs (Fig. 3) are not heavily obscured in the L-band. As a consequence, no strong absorption feature is present, and the continuum emission is due to the direct emission of the hot circumnuclear dust heated by the optical/UV primary AGN emission. In these cases, the AGN component dominates in the L band even when a significant starburst contribution to the bolometric luminosity is present. This is due to the \sim two order of magnitudes higher L-band/bolometric ratio in AGN than in starbursts. As a consequence, the PAH emission feature at $3.3 \mu\text{m}$ is either weak or absent.

- ($\Gamma > 1, \tau_{3.4} > 0.3$) AGNs are heavily obscured in the L-band. The observed continuum is the result of a strong dust extinction by dust. The heavy dust obscuration results into a highly reddened continuum (high Γ) and a strong absorption feature at $3.4 \mu\text{m}$. Since the AGN continuum is heavily absorbed, if a starburst is contributing to the bolometric luminosity, it is possible that it also represents a significant fraction of the L-band emission, depending on the amount of AGN extinction. This explains the wide range of measured values of the equivalent width of the $3.3 \mu\text{m}$ emission feature in these objects.

A more quantitative treatment of the relative star-

burst/AGN emission in ULIRGs will be discussed in the next Section 6.3.

With regard to starburst dominated sources, the observed spread in the L-band spectral parameters (continuum slope Γ , $EW_{3.3}$) is much smaller than in sources known to host an AGN. This spread could be either intrinsic (due to the age of the stellar populations) or due to an AGN component which has not been revealed through our indicators. For example, an unobscured or moderately obscured AGN contributing $\sim 1/3$ of the L-band emission would probably be missed by our analysis, and would imply a change by $\sim 30\%$ of the measurements of the above spectral parameters. We note that in order to have such a case the contribution of the AGN to the bolometric luminosity has to be negligible (of the order of a percent or smaller).

Finally, we cannot exclude that a powerful AGN, even dominating the bolometric luminosity, with a high enough obscuration to make negligible its contribution in the L-band, is present in some of the starburst-classified ULIRGs. In this case the only affected parameter would be the L-band to bolometric ratio. Given the large spread in this parameter, (Fig. 4) even among starburst-classified sources alone, this possibility cannot be excluded for any of the sources in our sample.

6.3 The AGN contribution to ULIRGs

Estimating the relative contribution of AGNs to the luminosity of ULIRGs is a more ambitious goal than the simple detection of AGNs inside ULIRGs. A multi-wavelength analysis, based on models of the whole optical to FIR Spectral Energy Distribution (SED) is probably the most powerful approach to this problem. Such a study for several of our sources is currently being finalized (Fritz et al. 2005, in prep.).

Here we only focus on L-band diagnostics.

Our analysis of the AGN contribution to ULIRGs luminosity is done in two steps: (a) estimate of the fraction of ULIRGs hosting an AGN; (b) estimate of the relative AGN/starburst contribution to the total luminosity in sources hosting an AGN.

6.3.1 Fraction of ULIRGs hosting AGNs

Out of the 14 ULIRGs in Table 5, only 5 do not show any evidence for the presence of an AGN. These sources belong to the flux-limited sample defined by the criterion $S_{60} > 5.24$ Jy (Sect. 2). In order to complete this sample only two objects are missing: IRAS 15250+3609 and IRAS 22491-1808. The first one has never been observed in the L-band, while the second one was not detected in our ISAAC observation. Both sources have been observed in the X-rays with *XMM-Newton* (Franceschini et al. 13), and in the mid-IR with ISO (G98), and no indication of the presence of an active nucleus has been found in both cases. Therefore, in order to be conservative in the estimate of the fraction of AGN-hosting ULIRGs, we classify these two sources as starburst-dominated. The final sample of 16 ULIRGs consists of 7 starburst dominated objects (44%) and 9 objects with a significant AGN contribution (56%).

These results have been obtained by using a flux selection at $60 \mu\text{m}$. This is not an unbiased selection criterion,

because of the higher fraction of bolometric luminosity emitted at 60 μm by starbursts with respect to AGNs (see also the discussion in Risaliti et al. 41). In our sample the average fraction of the total IR luminosity emitted at 60 μm (using Eq. 1) is 0.62 for the seven starbursts, and 0.52 for the 9 AGNs. This implies that in order to have the same total IR flux limit for AGNs and starbursts, the flux limit at 60 μm must be lower for AGNs by a factor (0.62/0.52=1.19). Assuming a euclidean logN-logS, the expected correction for the number of AGNs in a 60 μm flux limited sample is $1.19^{3/2}=1.30$. When this correction is taken into account, the final estimate of the fraction of ULIRGs hosting an AGN is 63%.

6.3.2 Deconvolution of the AGN and starburst components

An accurate estimate of the relative starburst/AGN contribution for each source in the L-band requires a spectral decomposition of the two components. This is extremely difficult due to the spread of intrinsic properties shown in Fig. 3 and 4.

A zeroth-order indicator of the relative contribution of the two components is the logarithmic ratio R_L^{corr} between the absorption-corrected continuum luminosity in the L-band and the total IR luminosity (Fig. 3b). It is shown in Fig. 3b that sources whose L-band spectrum is dominated by the unobscured emission of an AGN have $R_L^{\text{corr}} > -1$, while the average value for starburst-dominated sources is $R_L^{\text{corr}} \sim -2.6$. For comparison, $R_L = -0.57$ in the quasar spectral energy distribution of (11). The huge difference between the two values of R_L^{corr} for starbursts and AGNs, and the relatively large dispersion around the average values makes an accurate estimate of the relative contributions of the two components extremely difficult. For example, if 50% of the total IR luminosity of a ULIRG hosting an unobscured AGN is due to a circumnuclear starburst, R_L^{corr} would be changed only by a factor of two, well within the spread shown in Fig. 3b. The conclusion is that the L-band spectrum of ULIRGs hosting an unobscured AGN is dominated by the AGN emission even if the starburst is the dominant energy source.

The situation is significantly different for obscured AGNs. In these cases dust extinction of a few magnitudes can make the AGN emission comparable to that of a starburst of similar bolometric luminosity. The continuum extinction can be estimated from the measured 3.4-4 μm slope.

In order to quantitatively estimate these contributions, we made several assumptions on the intrinsic AGN and starburst emission, and developed a simple model to reproduce the observed L-band spectra. The main features of the model are the following:

- The observed L-band spectra are the composition of AGN and starburst contributions, which are parametrized as:

$$f_\lambda = \alpha f_{\lambda, \text{AGN}} e^{-\tau_L(\lambda)} + (1 - \alpha) f_{\lambda, \text{SB}} \quad (2)$$

where α is the fraction of the L-band luminosity due to the AGN, and $\tau_L(\lambda)$ is the wavelength dependent continuum optical depth in the L-band. $f_{\lambda, \text{AGN}}$ and $f_{\lambda, \text{SB}}$ are the intrinsic AGN and starburst L-band spectra.

- Based on the results of the spectral analysis shown in Table 3 and 4, and in Figure 3 and 4, we assume $f_{\lambda, \text{AGN}} = \lambda^{-0.5}$ and $f_{\lambda, \text{SB}} = \lambda^{-0.5} + f_{\text{PAH}}$. f_{PAH} is the contribution of the 3.3 μm emission feature, normalized in order to have $EW_{3.3, \text{SB}} = 110 \text{ nm}$ with respect to the pure starburst continuum. The choice of the spectral index ($\Gamma = -0.5$ for both pure AGN and pure starburst) has been driven by the average values observed in our sample, both for starburst-dominated and AGN-dominated ULIRGs. The value for AGNs is in agreement with L-band spectra of pure type 1 AGNs (Imanishi & Wada 21). The value for starbursts is the average from our data, and has a large scatter (Fig. 3a). However, this uncertainty is not a major problem for our model (see details below). We note that our pure starburst spectra differ on average from the average spectra of lower luminosity normal galaxies (which have $\Gamma \sim -2$, Lu et al. 27), probably due to a larger contribution by hot dust in powerful starbursts.

- We assume an extinction law $\tau_L(\lambda) \propto \lambda^{-1.75}$ (7).

The model has two free parameters: τ_L and α , where $\tau_L = \tau_L(\lambda = 3.5 \mu\text{m})$. For each pair of these parameters we compute the slope, Γ , and the PAH feature equivalent width, $EW_{3.3}$, for the composite spectrum. A good analytic approximation (within a few percent) of these relations can be obtained noting that the wavelength interval (λ_1, λ_2) used for the continuum fit is rather narrow ($\lambda_1 \sim 3.4 \mu\text{m}$, $\lambda_2 \sim 4 \mu\text{m}$). Using a first order expansion in $\delta = (\lambda_2 - \lambda_1)/\lambda_1$ we easily obtain:

$$EW_{3.3} = \frac{(1 - \alpha)EW_{3.3, \text{SB}}}{\alpha e^{-\tau_L} + (1 - \alpha)} \quad (3)$$

$$\Gamma = -0.5 + \frac{1.75\tau\alpha e^{-\tau_L} + (1 - \alpha)}{\alpha e^{-\tau_L} + (1 - \alpha)} \quad (4)$$

We plot the results in Fig. 5. The two groups of curves are obtained freezing one of the two parameters and varying the other. Therefore, they form a grid which can be directly used to estimate the relative AGN contribution and the AGN L-band extinction of each single ULIRG.

Equations 3 and 4 can be easily solved in terms of α and τ_L . A quantitative analysis of the results is shown in the Appendix. Here we concentrate on a visual analysis of Fig. 5, from which both the strengths and the limitations of the model clearly emerge:

- It is possible to estimate with good accuracy the AGN contribution to the L-band emission in a large region of the parameter space ($\alpha > 0.1$, $\tau_L < 4$).
- Our diagnostics fails around the pure starburst region, where all the model lines converge and high degeneracy among the parameters is present. Therefore, we cannot exclude that L-band starburst-dominated objects host a heavily buried ($\tau_L > 5$) AGN. However, in the cases where the AGN dominates, it is still possible to disentangle its contribution even in highly obscured objects, such as IRAS 20551-4250 and UGC 5101 (numbers 7 and 8 in Fig. 5).
- The dependence on the choice of the intrinsic AGN and SB spectra is not strong: if, for example, the “pure starburst” point is moved (provided that it remains inside the starburst region of the plot), the only affected region is the one close to the point itself, where the model lines converge and the estimate of the parameters is not reliable. These limitations

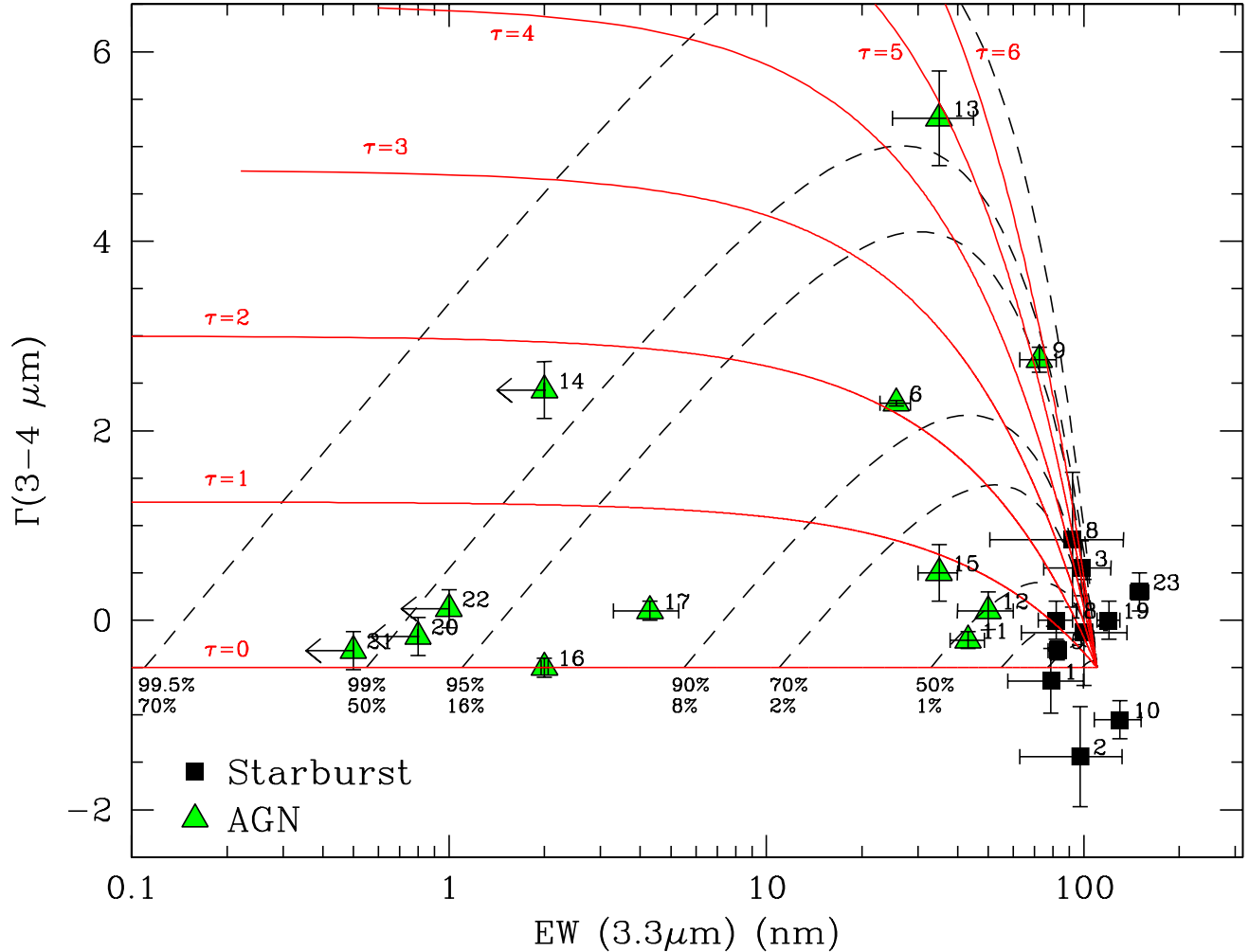


Figure 5. Estimates of the relative AGN/SB contribution in a L-band continuum slope versus $EW_{3.3}$ plot, according to the model described in the text. Dashed black lines represent combinations of AGN and SB with a fixed relative contribution with a varying L-band absorption of the AGN component (from $\tau_L = 0$ to $\tau_L = 6$). The two numbers below each line are the fractions (in percent) of the AGN contribution to the L-band (first number) and to the bolometric emission (second number). Continuous red lines represent combinations with a fixed AGN absorption (as labeled for each line) and a varying relative contribution. Following a dashed line from the bottom-left, it starts from a no-absorption point and moves to the upper-right direction as absorption (i.e. reddening AND attenuation of the AGN component) increases. It then moves to the lower right direction because as the reddening further increases, the starburst contribution becomes more important than the absorbed AGN component. Following a continuous line, it starts from a right point representing a pure AGN, and then moves to the bottom-left as the starburst contribution increases.

Numbers identifying each source refer to Table 6.

are quantitatively discussed in the Appendix, through the analysis of the statistical errors in the model.

6.3.3 AGN/SB contributions to the bolometric luminosity

A further step can be made estimating the AGN contribution to the bolometric luminosity. This is possible taking into account the different L-band to bolometric corrections for AGN and starbursts, $R_L(AGN)$ and $R_L(SB)$. We introduce a new parameter, K , defined as the ratio between the two bolometric corrections. From the considerations made above ($R_L(SB) \sim -2.6$, $R_L(AGN) \sim -0.6$) we have $K \sim 100$.

The fraction of the bolometric luminosity due to the AGN, α_{BOL} , is then given by

$$\alpha_{BOL} = \frac{\alpha}{\alpha + K(1 - \alpha)} \quad (5)$$

We list the results of the $(\alpha, \alpha_{BOL}, \tau_L)$ estimates in Table 6. Restricting our analysis on the complete sample (i.e. neglecting the five “control sources”) and adding up the contributions of both nuclei in the double sources, we obtain that the relative AGN contribution to the bolometric luminosity, α_{BOL} , is higher than 50% for 2 out of 9 AGNs. Correcting for incompleteness as explained in Section 6.4.1, we end up with the following conclusions:

- Fraction of sources with only a starburst component detected: $\sim 40\%$;
- Fraction of sources with a dominant starburst component and a minor AGN component $\sim 30\%$;
- Fraction of sources dominated by an AGN: $\sim 30\%$.

Simply averaging the AGN and starburst components we find that the overall contribution of starbursts to the

N	Source	$\alpha(\%)$	$\alpha_{BOL}(\%)$	τ_L	$\tau_L(\tau_{3.4})$	N	Source	$\alpha(\%)$	$\alpha_{BOL}(\%)$	τ_L	$\tau_L(\tau_{3.4})$
1	IRAS 12112+0305SW	0	0	—	—	13	UGC 5101	99±1	68±29	4.6±0.9	7.8±2.6
2	IRAS 12112+0305NE	0	0	—	—	14	IRAS 08572+3915	99.5±0.5	75±23	1.7±0.2	10.8±3.6
3	IRAS 14348-1447S	0	0	—	—	15	MKN 273	79±8	4±1	0.6±0.2	—
4	IRAS 14348-1447N	0	0	—	—	16	MKN 231	98±0.5	35±2	< 0.05	—
5	IRAS 17208-0014	0	0	—	—	17	IRAS 05189-2524	97±1	26±6	0.3±0.06	0.5±0.2
6	IRAS 19254-7245S	96±1	18±3	1.9±0.1	9.6±3.2	18	Arp 220	0	0	—	—
7	IRAS 19254-7245N	0	0	—	—	19	NGC 253	0	0	—	—
8	IRAS 20100-4156	0	0	—	—	20	MKN 463	99±1	62±26	0.2±0.1	1.4±0.4
9	IRAS 20551-4250	97±3	28±30	4.3±1.1	3.6±1.6	21	IRAS 20460+1925	99.5±0.5	71±23	0.1±0.1	—
10	IRAS 23128-5919S	58±8	1.5±0.5	< 0.2	—	22	IRAS 23060+0505	99±1	61±27	0.3±0.1	—
11	IRAS 23128-5919N	0	0	—	—	23	IC 694	0	0	—	—
12	NGC 6240	58±15	1.5±0.5	0.2 ^{+0.3} _{-0.2}	—						

Table 6. Relative AGN contribution to the L-band luminosity (α) and to the total bolometric luminosity, α_{BOL} , and L-band optical depth for the AGN component, τ_L , for the complete sample (first 18 sources) and for the control sources (last 5 sources), as estimated with the model described in Section 6.4.2, using the equations in Appendix. The second estimate of the continuum L-band optical depth, $\tau_L(\tau_{3.4})$, is based on the optical depth $\tau_{3.4}$ of the 3.4 μm absorption feature, according to a standard extinction curve (Pendleton et al. 1994). Quoted errors are due to measurement uncertainties only. Systematic effects maybe relevant in α_{BOL} (of the same order as statistical ones for AGN-dominated sources, and 2-3 times larger for starburst-dominated sources).

luminosity of ULIRGs is $\sim 75\%$, while the AGN contribution is the remaining 25% . Considering that the typical errors in estimating α in Fig. 5 vary from a few percent to $\sim 50\%$, and the propagation of errors in the computation of the average, we estimate the statistical uncertainty on the total averages to be of the order of 5-10%.

However, the determination of α_{BOL} has several caveats which must be taken into account. While the main uncertainties in the determination of α and τ are due to measurement errors, other systematic effects may be relevant, or even dominant. In particular, two possible complications must be considered:

(i) A completely hidden component, either AGN or starburst, due to heavy obscuration in the L-band, cannot be excluded. This would imply a contribution to the bolometric luminosity from the FIR, with no indications in the L-band. Such a scenario has been proposed for instance by Fischer (12) and Imanishi, Dudley, & Maloney (17) to explain the dependence of the PAH-to-FIR flux ratio with luminosity in starbursts: lower ratios are observed in higher luminosity sources, suggesting the presence of an obscured component. In order to test this scenario, we compared the total luminosity predicted with our model (and therefore based on the observed L-band components) with the FIR luminosities measured by IRAS. The results, plotted in Fig. 6 show that in most cases the two values match, suggesting that hidden components do not represent an important contribution to the bolometric luminosity. However, several points are significantly off the 1:1 relation. In these cases a contribution from a completely obscured component cannot be ruled out. Moreover, while the bolometric correction used for AGN is independently determined (Elvis et al. 1994), the L-band to FIR ratio for starbursts is inferred from our sample (Fig. 3b). Therefore, if a completely obscured component is responsible of a fraction of the FIR emission, we are implicitly assuming that it consists of a pure starburst. As a consequence, our estimates of the AGN contribution could actually be lower limits in some cases.

(ii) The spread in the L-band to bolometric ratio, both in starbursts and in AGNs (Fig. 3b) makes the determina-

tion of the parameter K rather uncertain. Moreover, the assumed average ratio for AGNs is that obtained from a sample of quasars (Elvis et al. 11) which could be significantly different from that of AGN-dominated ULIRGs, due to possible different amounts of circumnuclear dust. Taking into account this uncertainty, we conservatively estimate a range for K from ~ 30 to ~ 300 . By propagating the error on Equation 5 we obtain that this is the dominant uncertainty on α_{BOL} , at least for the sources not dominated by the AGN contribution in the L-band. For example, in the cases of NGC 6240 and IRAS 23128-5919S (Tab. 6) we obtain $\alpha_{BOL}(K=30)=3\%$, $\alpha_{BOL}(K=300)=0.3\%$. Note however that even assuming such large uncertainties, the basic result that in these sources the AGN total contribution is negligible still holds. We note that our result is not in agreement with that of Lutz et al. (30) who estimate an AGN contribution in the range 25-50%. This complex source will be discussed in more detail in a forthcoming paper (Risaliti et al. 43).

Summarizing the above analysis, we conclude that our simple model provides a reliable estimate of the relative AGN/starburst contribution for statistical purposes, with possible exceptions in single sources due to heavily obscured AGN or starburst components.

6.3.4 Comparison with previous results

Restricting our analysis on the complete sample made of the ULIRGs listed in Table 6 (14 sources, 4 with resolved double nuclei) we note that an AGN was found in 9 cases. In two cases the AGN is the dominant contribution to the bolometric luminosity, while in the other 7 cases the starburst is dominant. In the following we compare these results with the classification provided by studies at other wavelengths (Table 5):

- **X-rays:** the classification is in all cases in agreement with the results of X-ray spectroscopy.
- **Mid-IR:** the mid-IR analysis of G98, based on coronal lines and PAH emission features in ISO spectra, is in agreement with our conclusions for the five starburst

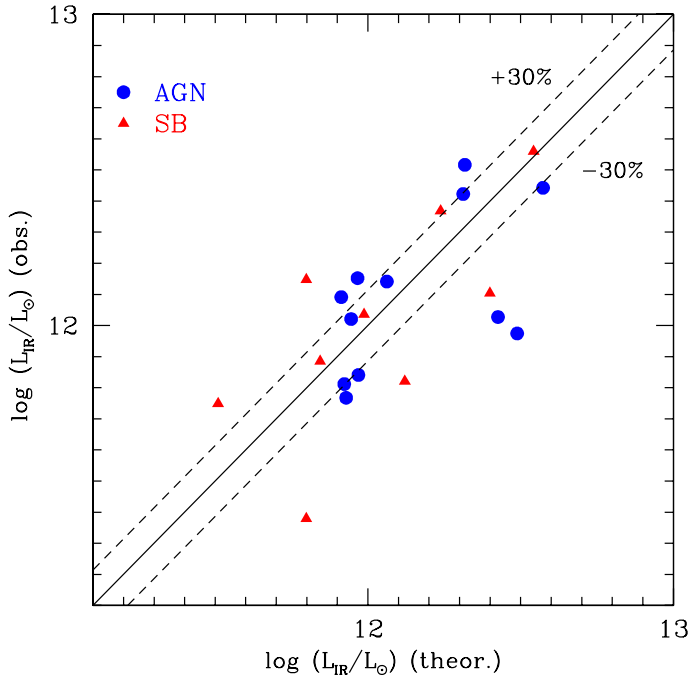


Figure 6. Comparison between the total infrared luminosity inferred with our model from the observed L-band emission, assuming standard bolometric corrections (see text for details), and the luminosity measured by IRAS.

ULIRGs. Signatures of an AGN are clearly found in two sources (MKN 231, MKN 273). One source (IRAS 05189-2524) is not in the G98 sample. One source (IRAS 19254-7245) show marginal evidence of the presence of an AGN (its position in the diagnostic diagrams is “half way” the starburst and AGN regions, but a reanalysis of Charmandaris et al. (2003) show clear evidence of the AGN). The remaining four sources (IRAS 20551-4250, UGC 5101, IRAS 23128-5919, NGC 6240) are classified as pure starbursts.

• **Optical/Near-IR:** spectral evidence of the presence of an AGN was found in four sources. All other objects have a starburst/LINER classification. Among them, the objects with an L-band detected AGN are NGC 6240, IRAS 20551-4250, IRAS 23128-5919, UGC 5101.

Summarizing, the above comparison shows that only L-band and hard X-ray spectroscopy is effective in finding evidence of AGNs in starburst-dominated and/or heavily absorbed ULIRGs, while the analysis at other wavelength fails in several cases.

This result can be easily explained comparing the fractions of *L-band* luminosity due to AGN, α , and the fraction of *bolometric* luminosity due to AGN, α_{BOL} (Table 6): in ALL cases where an AGN is present, its contribution to the L-band emission is dominant, even if this is not the case for the bolometric emission in 7 out of 9 cases. The same consideration applies to the hard X-ray band ($E > 2$ keV), due to the much higher fraction of bolometric luminosity emitted in the X-rays by AGNs (several percent) than by starbursts ($< 10^{-4}$), but not to any other spectral region:

- at wavelengths between the hard X-rays and 2-5 μ m the AGN emission is in almost all cases completely absorbed by

dust;

- at wavelengths higher than a few micron the AGN emission is diluted by the dominant starburst emission.

Concluding, the L-band and hard X-ray spectroscopy are the best spectral regions in order to investigate the energy source in ULIRGs. As pointed out in Section 6.1, the X-ray band analysis is limited to a handful sources with the current instrumentation. Therefore, L-band spectroscopy is the most promising way to extend our understanding of the AGN/starburst nature of ULIRGs in larger samples. We stress again that the diagnostics developed here has been suggested by the analysis of our high quality ISAAC spectra, but once calibrated does not require particularly high signal-to-noise data, and is capable to solve cases which were not easily understandable in previous analyses. A particularly striking example is the luminous infrared galaxy NGC 4418 ($L_{IR} = 10^{11.2} L_\odot$), which show clear signatures of the presence of an AGN in the mid-IR (Dudley & Wynn-Williams 10, Spoon et al. 51), but not in the L-band, according to Imanishi et al. (22). However, when our diagnostic diagrams (Fig. 3a and 3b) are applied to its L-band spectrum, we find that it clearly lays in the AGN region. Our model indicates an interpretation similar to that for IRAS 20551-4250, with a heavily buried AGN ($\tau \sim 3-4$) and a starburst component responsible for $\sim 70\%$ of the bolometric luminosity.

6.4 Composition of the circumnuclear medium in ULIRGs

We already noticed that the correction used to estimate the intrinsic L-band luminosity in heavily obscured AGNs, based on the optical depth of the 3.4 μ m absorption feature, leads to values $\log R_L^{corr} > 0$ for three out of the 4 sources with $\tau_{3.4} > 0.3$. In particular, we obtain $\log R_L^{corr} = 2.7$ for IRAS 19254-7245, $\log R_L^{corr} = 3.2$ for IRAS 08572+3915, $\log R_L^{corr} = 2.3$ for UGC 5101. These unphysically high values can be discussed considering their relation (a) with the L-band continuum optical depth τ_L estimated with the model presented in the previous Section, and (b) with the gas absorption measured in the X-rays.

(a) The high optical depth of the 3.4 μ m absorption features in three objects implies an L-band extinction of several magnitudes, assuming the standard absorption law of Pendleton et al. (36) ($A_L \sim 12 \pm 4\tau_{3.4}$). Even considering the lowest allowed value, i.e. $A_L = 8\tau_{3.4}$, we would still have an L-band to total infrared ratio $\log R_L^{corr} > 0$ for two sources (IRAS 19254-7245 and IRAS 08572+3915).

On the other hand, the extinction τ_L obtained from the spectral decomposition presented in the previous Section is significantly lower in the three objects with the highest $\tau_{3.4}$, and compatible with an intrinsic L-band to bolometric ratio $\log R_L^{corr} \sim 0$. The comparison between the two estimates of the optical depth is shown in Table 6.

The above results imply that the abundance of hydrocarbon dust grains, responsible for the 3.4 μ m absorption, is on average higher in these ULIRGs than in the Galactic ISM. This is the case for all the three sources with strong absorption at 3.4 μ m ($\tau_{3.4} \sim 0.8 - 0.9$). We note that this is not necessarily a general feature in ULIRGs, since selection effects could play a role: such high $\tau_{3.4}$ can be observed only in objects where the dust grains responsible of the 3.4 μ m absorption are overabundant, because otherwise the contin-

uum extinction would be so high to prevent the AGN emission from being observable.

(b) The column density measured in the X-rays are $N_H > 10^{24} \text{ cm}^{-2}$ for UGC 5101 and IRAS 19254-7245, based on the *XMM-Newton* observations (Imanishi et al. 20 and Braito et al. 5) and $N_H > 10^{25} \text{ cm}^{-2}$ for IRAS 08572+3915 from a BeppoSAX observation (Risaliti et al. 2005, in prep.). Assuming a standard Galactic extinction curve and dust-to-gas ratio (Savage & Mathis 48) we have $A_L \sim 1.2 N_{H,23}$, where $N_{H,23}$ is the column density in units of 10^{23} cm^{-2} . This would imply $A_L > 12$ for UGC 5101 and IRAS 19254-7245, and $A_L > 120$ for IRAS 08572+3915. Again, these values are not acceptable, because they would imply a too high intrinsic continuum. We conclude that the dust-to-gas ratio in heavily obscured ULIRGs is at least a factor of a few smaller than in the Galactic ISM. This is a well known property of the absorbing medium in Seyfert Galaxies with moderate absorption, i.e. $N_H < 10^{23} \text{ cm}^{-2}$ (Maccacaro, Perola, & Elvis 32, Maiolino et al. 31). Here we find that this is also the case for higher luminosity and higher column density AGNs.

7 CONCLUSIONS

In this paper two works are presented: (1) L-band spectra obtained with ISAAC at VLT are analyzed for a sample of 7 Ultraluminous Infrared Galaxies, and (2) a detailed discussion on L-band diagnostics for ULIRGs is performed, using a complete sample of local bright ULIRGs, obtained merging our observations with the available L-band spectra of sources in the northern hemisphere.

1. The spectral analysis of the sample of 7 bright southern ULIRGs show the power of ISAAC in revealing the nature of these objects. Six sources are known to have double nuclei. In four cases we obtained a spectrum for both nuclei. A clear signature of the presence of an AGN was found in three nuclei (IRAS 19254-7245S, IRAS 20551-4250, IRAS 23128-3915S). In two of these three objects (IRAS 19254-7245A, IRAS 20551-4250) an absorption feature at $3.4 \mu\text{m}$, due to hydrocarbon dust absorption was detected. These two sources have also the steepest continuum ($\Gamma > 2$). Water ice absorption at $3.1 \mu\text{m}$ was also detected in several objects. We confirm that $3.4 \mu\text{m}$ absorption is a typical signature of an AGN, while $3.1 \mu\text{m}$ absorption with moderate optical depths ($\tau_{3.1} < 0.5$) is found in sources with no indication of an active nucleus.

The high quality of the spectra obtained with ISAAC demonstrates that L-band spectroscopy can be a powerful tool to investigate the nature of relatively faint ULIRGs. For example, most of the 118 sources of the 1 Jy sample (Kim & Sanders 24) are probably bright enough for such a study. This is not true for studies at other wavelengths, such as in the X-rays, which are in principle extremely effective in disentangling AGNs and starbursts but can only be performed with the 10/15 brightest sources with the currently available instrumentation.

2. We performed a complete analysis of the L-band spectral diagnostics on a sample consisting of our seven southern ULIRGs, 7 northern ULIRGs selected with the same criterion ($60 \mu\text{m}$ flux density $S_{60} > 5.2 \text{ Jy}$) and 5 more sources which are known to be either AGN-dominated or starburst

dominated, with a slightly lower bolometric luminosity. All these sources have a reliable, independent starburst/AGN classification based on observations at other wavelengths. The main results are the following:

- In all known AGN, *at least* one L-band AGN indicator is detected, while no AGN indicators are found in any object classified as starburst. However, no single indicator provides a 100% correct classification.
- When more indicators are combined, a 100% correct starburst/AGN classification is possible. We found that AGNs and starbursts are completely separated in two different bi-dimensional diagrams, the first obtained plotting the $3.5\text{-}4 \mu\text{m}$ continuum slope, Γ , versus the $3.3 \mu\text{m}$ PAH emission feature equivalent width, $EW_{3.3}$; the second plotting $EW_{3.3}$ versus the extinction-corrected L-band to bolometric emission ratio.
- ULIRGs hosting AGNs can be clearly separated into two groups. The first consists of objects where the AGN is not heavily absorbed in the L-band. The continuum is dominated by the re-emission by hot dust of the AGN direct emission; the continuum slope (in a $\lambda - f_\lambda$ plane) is flat; the PAH emission feature is weak or absent; absorption features are absent. The second group is made by objects heavily absorbed in the L-band. In these cases the emission is dominated by the reprocessing by cold dust. The continuum is steep ($\Gamma \sim 2$) due to reddening, and strong absorption features are present.
- We use a simple model for the spectral deconvolution of the AGN and starburst components. We show that it is possible to estimate the relative AGN and starburst contributions to the bolometric luminosity through L-band spectral indicators.
- The application of our model to a representative sample of ULIRGs in the local Universe shows that AGNs are present in $\sim 60\%$ of ULIRGs. In about half of these cases the AGN contribution to the bolometric luminosity is dominant. Overall, the AGN contribution to the ULIRG luminosity in the local Universe is $\sim 30\%$, the remaining 70% being due to starburst emission.
- The comparison between gas absorption (from X-ray observations), continuum extinction in the L-band, and the narrow absorption feature at $3.4 \mu\text{m}$ suggest that heavily obscured ULIRGs have a low dust-to-gas ratio and a different extinction curve with respect to the Galactic ISM. In particular, hydrocarbon dust grains are overabundant in three out of four cases with respect to the Galactic dust composition.

ACKNOWLEDGMENTS

We are grateful to Loredana Bassani for her contribution to the early stage of this project, and to the anonymous referee for very useful comments. This publication makes use of data products from the Two Micron All Sky Survey, which is a joint project of the University of Massachusetts and the Infrared Processing and Analysis Center/California Institute of Technology, funded by the National Aeronautics and Space Administration and the National Science Foundation. Also, we made use of the NASA/IPAC Extragalactic Database (NED) which is operated by the Jet Propulsion Laboratory, California Institute of Technology, under con-

tract with the National Aeronautics and Space Administration.

APPENDIX A: ANALYSIS OF THE AGN/SB DECONVOLUTION MODEL

The relations plotted in Fig. 5, and expressed in Equations 3 and 4 can be inverted in order to work out the explicit dependence of the two model parameters, α and τ_L , on the observed parameters, EW and Γ :

$$\tau_L = \frac{EW_{SB}\Gamma - EW}{\beta(EW_{SB} - EW)} \quad (A1)$$

$$\alpha = \frac{EW_{SB} - EW}{(EW_{SB} - EW) + EW * e^{-\tau_L}} \quad (A2)$$

where $\beta = 1.75$ is the slope of the extinction curve in the L-band, EW_{SB} is the intrinsic equivalent width of the $3.3 \mu\text{m}$ PAH feature in a pure starburst spectrum.

From these two equations we obtain the errors on τ_L and α :

$$\Delta\tau_L = \frac{EW}{EW_{SB} - EW} \frac{|\Gamma - 1|\Delta(EW)}{\beta(EW_{SB} - EW)} + \frac{\Delta(\Gamma)}{\beta} \quad (A3)$$

$$\Delta\alpha = \frac{\alpha^2 e^{-\tau_L}}{EW_{SB} - EW} EW \Delta(\tau_L) + \frac{EW_{SB} \Delta(EW)}{EW_{SB} - EW} \quad (A4)$$

where $\Delta(EW)$ and $\Delta(\Gamma)$ are the errors on our measurements.

These equations have been used to estimate the errors in Table 6. Moreover, they can be analyzed in order to quantitatively estimate in which regions of the (EW, Γ) parameter space we can measure the relative SB/AGN contribution with good precision. In Fig. A1 we plot the relative errors, $\Delta(\tau_L)/\tau_L$ and $\Delta(EW)/EW$ versus the measured EW , for different values of Γ , and assuming $\Delta(\tau_L)/\tau_L = 0.1$ and $\Delta(EW)/EW = 0.2$.

The regions with a bad determination of α (with errors higher than 50%) are those with high equivalent width of the $3.3 \mu\text{m}$ emission feature and a steep spectrum, corresponding to the upper right region in Fig. 5 where the model lines get closer while approaching the pure starburst point. This is also clear from Eq. A4, where the value of $\Delta\alpha$ diverges for $EW \rightarrow EW_{SB}$.

REFERENCES

Allamandola L. J., Tielens G. G. M., Barker J. R., 1989, ApJS, 71, 733
 Alonso-Herrero A., Ward M. J., Kotilainen J. K., 1997, MNRAS, 288, 977
 Armus L., et al., 2004, ApJS, 154, 178
 Berta S., Fritz J., Franceschini A., Bressan A., Pernechele C., 2003, A&A, 403, 119
 Braito V., et al., 2003, A&A, 398, 107
 Braito V., et al., 2004, A&A, 420, 79
 Cardelli J. A., Clayton G. C., Mathis J. S., 1989, ApJ, 345, 24
 Charmandaris V., et al., 2002, A&A, 391, 429
 Duc P.-A., Mirabel I. F., Maza J., 1997, A&AS, 124, 533
 Dudley C. C., Wynn-Williams C. G., 1997, ApJ, 488, 720
 Elvis M., et al., 1994, ApJS, 95, 1
 Fischer J., 2000, ibp..conf, 239
 Franceschini A., et al., 2003, MNRAS, 343, 1181
 Genzel R., et al., 1998, ApJ, 498, 579 (G98)
 Imanishi M., Dudley C. C., 2000, ApJ, 545, 701
 Imanishi M., 2000, MNRAS, 319, 331
 Imanishi M., Dudley C. C., Maloney P. R., 2001, ApJ, 558, L93
 Imanishi M., 2002, ApJ, 569, 44
 Imanishi M., Maloney P. R., 2003, ApJ, 588, 165
 Imanishi M., Terashima Y., Anabuki N., Nakagawa T., 2003, ApJ, 596, L167
 Imanishi M., Wada K., 2004, ApJ, 617, 214
 Imanishi M., Nakanishi K., Kuno N., Kohno K., 2004, AJ, 128, 2037

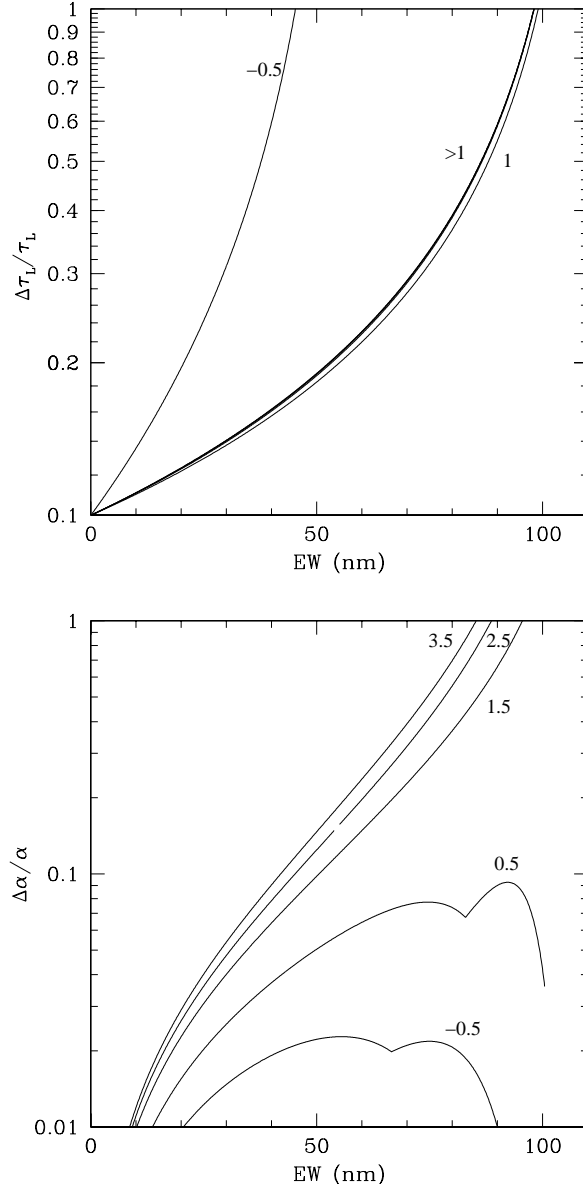


Figure A1. Relative errors on τ_L (upper panel) and α (lower panel) versus the observed equivalent width of the $3.3 \mu\text{m}$ emission feature, for different values of the observed Γ . The value of Γ is labeled in each line.

Imanishi M., Dudley C. C., Maloney P. R., 2005, *ApJ*, accepted (astro-ph/0509861)

Iwasawa K., Sanders D. B., Evans A. S., Trentham N., Miniutti G., Spoon H. W. W., 2005, *MNRAS*, 357, 565

Kim D.-C., Sanders D. B., 1998, *ApJS*, 119, 41

Kim D.-C., Veilleux S., Sanders D. B., 2002, *ApJS*, 143, 277

Laureijs R. J., et al., 2000, *A&A*, 359, 900

Lu N., et al., 2003, *ApJ*, 588, 199

Lutz D., Veilleux S., Genzel R., 1999, *ApJ*, 517, L13

Lutz D., Maiolino R., Moorwood A. F. M., Netzer H., Wagner S. J., Sturm E., Genzel R., 2002, *A&A*, 396, 439

Lutz D., Sturm E., Genzel R., Spoon H. W. W., Moorwood A. F. M., Netzer H., Sternberg A., 2003, *A&A*, 409, 867

Maiolino R., Marconi A., Salvati M., Risaliti G., Severgnini P., Oliva E., La Franca F., Vanzi L., 2001, *A&A*, 365, 28

Maccacaro T., Perola G. C., Elvis M., 1982, *ApJ*, 257, 47

Mason R. E., Wright G., Pendleton Y., Adamson A., 2004, *ApJ*, 613, 770

Moorwood A. F. M., 1986, *A&A*, 166, 4

Ptak A., Heckman T., Levenson N. A., Weaver K., Strickland D., 2003, *ApJ*, 592, 782

Pendleton Y. J., Sandford S. A., Allamandola L. J., Tielens A. G. G. M., Sellgren K., 1994, *ApJ*, 437, 683

Pendleton Y. J., Allamandola L. J., 2002, *ApJS*, 138, 75

Pernechele C., Berta S., Marconi A., Bonoli C., Bressan A., Franceschini A., Fritz J., Giro E., 2003, *MNRAS*, 338, L13

Rigopoulou D., Spoon H. W. W., Genzel R., Lutz D., Moorwood A. F. M., Tran Q. D., 1999, *AJ*, 118, 2625

Risaliti G., Maiolino R., Salvati M., 1999, *ApJ*, 522, 157

Risaliti G., Gilli R., Maiolino R., Salvati M., 2000, *A&A*, 357, 13

Risaliti G., et al., 2003, *ApJ*, 595, L17

Risaliti G., et al., 2005, *ApJ*, in prep.

Sanders D. B., Soifer B. T., Elias J. H., Madore B. F., Matthews K., Neugebauer G., Scoville N. Z., 1988, *ApJ*, 325, 74

Sanders D. B., Mirabel I. F., 1996, *ARA&A*, 34, 749

Sanders D. B., Mazzarella J. M., Kim D.-C., Surace J. A., Soifer B. T., 2003, *AJ*, 126, 1607

Sandford S. A., Allamandola L. J., Tielens A. G. G. M., Sellgren K., Tapia M., Pendleton Y., 1991, *ApJ*, 371, 607

Savage B. D., Mathis J. S., 1979, *ARA&A*, 17, 73

Severgnini P., et al., 2000, *A&A*, 360, 457

Spergel D. N., et al., 2003, *ApJS*, 148, 175

Spoon H. W. W., Keane J. V., Tielens A. G. G. M., Lutz D., Moorwood A. F. M., 2001, *A&A*, 365, L353

Veilleux S., Kim D.-C., Sanders D. B., Mazzarella J. M., Soifer B. T., 1995, *ApJS*, 98, 171

Veilleux S., Kim D.-C., Sanders D. B., 1999, *ApJ*, 522, 113

Veilleux S., Sanders D. B., Kim D.-C., 1999, *ApJ*, 522, 139

Vignati P., et al., 1999, *A&A*, 349, L57

Voit G. M., 1992, *MNRAS*, 258, 841

Werner M. W., et al., 2004, *ApJS*, 154, 1